Finite-difference elastic anisotropic wave propagation

John T. Etgen

ABSTRACT

The heterogeneous anisotropic elastic wave equation can be solved on a discrete grid using an explicit finite-difference technique. This solution of the wave equation is used for forward modeling as well as for prestack migration of elastic wave fields. A three-dimensional version of the method can compute the elastic wave field in a heterogeneous anisotropic medium due to a variety of sources. For an axisymmetric-anisotropic 2-D medium, the equations that govern in-plane pseudo-P and pseudo-S_v waves are uncoupled from the S_h wave equation. The P–S_v and S_h wave fields excited by a line source can then be calculated on separate 2-D grids. The finite-difference method uses spatial differentiation operators centered halfway between grid points, and represents stresses and displacements on a staggered grid. For common descriptions of an anisotropic solid, no interpolation of grid values is needed during the computations. The wave fields in both solid and liquid media are computed using the same equations; layer boundaries are represented by changes in elastic constants throughout the computational grid without need for explicit boundary conditions. Absorbing boundaries are used to reduce undesirable edge effects. A free surface condition is also incorporated at the top of the model. Elastic wave fields calculated using the 3-D and 2-D versions of the algorithm agree with analytical solutions for simple Earth models. Wave fields in more complicated models with varying degrees of anisotropy and heterogeneity show expected behavior, although direct comparison with analytical solutions is impossible. For 3-D calculations, an efficient "out-of-core" algorithm computes multiple time steps on each pass through the computational model to reduce the i/o cost of the method. The algorithm is organized to deal with the data as a sequence of planes so the data does not have to be transposed during the computations.

INTRODUCTION

Acoustic isotropic models of the earth do not adequately model wave propagation in realistic cases. S waves and the presence of anisotropy can provide valuable information about the medium that seismic waves propagate through; this information is lost when only considering acoustic isotropic wave propagation. Allowing elastic wave propagation, and furthermore, removing the standard assumption of isotropy more accurately describes waves that propagate in the Earth. Finite-difference methods applied to the elastic wave equation provide one possible method for solving the complicated equations that govern wave propagation in an anisotropic solid. More realistic models of wave propagation will lead to a better understanding of the waves observed in the Earth and to more accurate methods of imaging the subsurface.

Many authors have addressed the propagation of waves in elastic media. Traditionally, however, finite-difference modeling of the elastic wave equation is usually limited to two-dimensional media and almost exclusively to isotropic media. Kelly et al., (1976), describe a simple finite-difference approximation to the elastic wave equation to model P and S_v waves in isotropic homogeneous and heterogeneous media. Several authors have suggested improvements to the finite-difference technique used for the elastic wave equation. Virieux (1984, 1986) describes a method that updates stresses and particle velocities on a staggered grid that overcomes the accuracy and stability problems of the non-centered standard finite-difference approximations of both the P–S_v wave equations and the S_h wave equation. Virieux's method is appropriate for 2-D isotropic heterogeneous media, including liquid layers. Although formulated using first order differences, Virieux's method could be extended to use more accurate difference approximations. Mora (1986a) described a finite-difference method that represents the stresses and displacements on a staggered grid similar to Virieux's that solves the isotropic elastic wave equation in two dimensions for P and S_v waves using accurate convolutional derivative operators. Kosloff et al. (1984, 1985), described a Fourier technique to solve the isotropic elastic wave equation in two and three dimensions. Spatial derivatives taken in the Fourier domain (accurate to about 2.5 points per highest wavelength) are more accurate than finite-difference spatial derivatives. For this reason the Fourier method seems ideal for 3-D calculations, but the convolutional operators designed by Mora are accurate to about 3 points per highest wavelength giving the Fourier method only a slight advantage in accuracy and storage. The need to access the computational data in transposed order is a disadvantage to the 3-D Fourier technique.

The finite-difference method presented here is based on the staggered grid and convolutional operators of Mora (1986a) but updates displacements in time instead of stresses. The method is designed to compute elastic wave fields in 3-D heterogeneous anisotropic solids. To simulate 2-D anisotropic elastic wave propagation an axisymmetric-anisotropic medium is assumed; the pseudo-P–pseudo-S_v wave equation is uncoupled from the S_h wave equation and can be solved on a separate 2-D

grid. The wave field amplitudes modeled by this 2-D procedure are accurate for a line source. Examples show that the method accurately propagates elastic waves in both isotropic and anisotropic media in both two and three dimensions. Values for elastic constants derived from rock samples show that waves in anisotropic media can exhibit exotic behavior.

ANISOTROPIC ELASTIC WAVE PROPAGATION

The seismic wave field in an anisotropic linearly-elastic lossless solid medium excited by a given source or sources can be computed by evolving forward in time with the elastic wave equation. A convenient form of the elastic wave equation used for time stepping is obtained from the equations relating strain and displacement, the stress-strain relation (Hooke's law), and the law of conservation of momentum. Starting from the relation between strains and displacements,

$$e_{ij} = \frac{1}{2}\Big(\frac{\partial U_i}{\partial x_j} + \frac{\partial U_j}{\partial x_i}\Big) \quad i,j = 1,3 \tag{1}$$

strains (e_{ij}) are computed from displacements (U_i). Using the stress strain relation for a general linear-elastic solid,

$$\sigma_{kl} = C_{ijkl} e_{ij} \quad i,j,k,l = 1,3 \tag{2}$$

the stresses (σ_{kl}) in the medium are computed. The constants C_{ijkl} describe the elastic properties of the medium, and ρ is the density of the medium. The quantities $e_{ij}, U_i, \sigma_{kl}, C_{ijkl}$, and ρ are functions of spatial position but for compactness sake the spatial dependence is suppressed here. Using the law of conservation of momentum, and substituting x, y, z for i, j, k,

$$\begin{aligned}
\frac{1}{\rho}\Big[\frac{\partial \sigma_{xx}}{\partial x} + \frac{\partial \sigma_{xz}}{\partial z} + \frac{\partial \sigma_{xy}}{\partial y} - F_x\Big] &= \frac{\partial^2 U_x}{\partial t^2} \\
\frac{1}{\rho}\Big[\frac{\partial \sigma_{yy}}{\partial y} + \frac{\partial \sigma_{zy}}{\partial z} + \frac{\partial \sigma_{xy}}{\partial x} - F_y\Big] &= \frac{\partial^2 U_y}{\partial t^2} \\
\frac{1}{\rho}\Big[\frac{\partial \sigma_{zz}}{\partial z} + \frac{\partial \sigma_{xz}}{\partial x} + \frac{\partial \sigma_{zy}}{\partial y} - F_z\Big] &= \frac{\partial^2 U_z}{\partial t^2}
\end{aligned} \tag{3}$$

the particle accelerations can be calculated. This representation of the elastic wave equation can then be solved for particle displacements at later times by integration.

Since particle rotation plays no part in wave propagation, the 3x3 matrix σ_{kl} must be symmetric; and e_{ij} is also symmetric. The elastic stiffness tensor C_{ijkl} must be symmetric and for energy conservation it must also be positive definite. This means for example that $\sigma_{kl} = \sigma_{lk}$, $e_{ij} = e_{ji}$ and $C_{ijkl} = C_{ijlk} = C_{jikl}$. In light of these properties it is useful to introduce another notation system for the quantities σ_{kl}, e_{ij}, and C_{ijkl}. Using x, y, z rather than i, j, k and setting

$1 \leftarrow xx$, $2 \leftarrow yy$, $3 \leftarrow zz$, $4 \leftarrow zy$, $5 \leftarrow xz$, and $6 \leftarrow xy$ the σ and e matrices become 6 element vectors and the stiffness tensor C becomes a 6x6 matrix. One can then write the stress-strain relation as follows:

$$\begin{pmatrix} \sigma_{xx} \\ \sigma_{yy} \\ \sigma_{zz} \\ \sigma_{zy} \\ \sigma_{xz} \\ \sigma_{xy} \end{pmatrix} = \begin{pmatrix} C_{11} & C_{12} & C_{13} & C_{14} & C_{15} & C_{16} \\ C_{12} & C_{22} & C_{23} & C_{24} & C_{25} & C_{26} \\ C_{13} & C_{23} & C_{33} & C_{34} & C_{35} & C_{36} \\ C_{14} & C_{24} & C_{34} & C_{44} & C_{45} & C_{46} \\ C_{15} & C_{25} & C_{35} & C_{45} & C_{55} & C_{56} \\ C_{16} & C_{26} & C_{36} & C_{46} & C_{56} & C_{66} \end{pmatrix} \begin{pmatrix} e_{xx} \\ e_{yy} \\ e_{zz} \\ e_{zy} \\ e_{xz} \\ e_{xy} \end{pmatrix}, \tag{4}$$

without loss of generality.

Axisymmetric and orthorhombic anisotropy

Because it is often difficult to obtain unique values for all 21 independent elastic constants C_{ijkl} for a generaly-anisotropic medium, it is worthwhile to consider classes of anisotropy described by fewer independent elastic constants. Axisymmetric anisotropy, described by 5 independent elastic constants, is a simpler form of anisotropy commonly used to describe shales or other layered rocks. In most cases, especially for shales, the vertical axis is take to be the axis of symmetry of the elastic stiffness matrix C. In this case, the rock is often called transversely isotropic because propagation velocity at a point in the medium does not depend on azimuth. Axisymmetric anisotropy is convenient because the equations that govern pseudo-P and pseudo-S_v wave propagation (hereafter referred to simply as P and S_v waves) are uncoupled from the equation that governs S_h wave propagation. If a medium with no cross-line variations excited by a line source is considered, a convenient 2-D method for wave propagation can be derived. In the general heterogeneous anisotropic case, 2-D computations are not possible because of the dependence of the medium on azimuth, and the coupling of all wave types.

If a given medium is not invariant in the cross-line direction, but is axisymmetric-anisotropic, wave field calculations are carried out in 3-D. The stress-strain relation for a 3-D axisymmetric-anisotropic medium can be written as,

$$\begin{pmatrix} \sigma_{xx} \\ \sigma_{yy} \\ \sigma_{zz} \\ \sigma_{zy} \\ \sigma_{xz} \\ \sigma_{xy} \end{pmatrix} = \begin{pmatrix} C_{11} & C_{12} & C_{13} & & & \\ C_{12} & C_{11} & C_{13} & & & \\ C_{13} & C_{13} & C_{33} & & & \\ & & & C_{44} & & \\ & & & & C_{44} & \\ & & & & & C_{66} \end{pmatrix} \begin{pmatrix} e_{xx} \\ e_{yy} \\ e_{zz} \\ e_{zy} \\ e_{xz} \\ e_{xy} \end{pmatrix} \tag{5}$$

with the constraint $C_{12} = C_{11} - C_{66}$. For this stiffness matrix to be positive definite (for energy conservation), the following constraints must also be satisfied.

$$C_{11} \geq C_{66} \geq 0 \;\; ; \;\; C_{33} \geq 0 \;\; ; \;\; C_{44} \geq 0 \;\; ; \;\; C_{13}^2 \leq C_{33}(C_{11} - \frac{1}{2}C_{66})$$

A 2-D version of the axisymmetric-anisotropic elastic wave equation can be derived by considering in-plane (constant y) propagation and separating the stresses, strains and components of the stiffness matrix that involve the y-direction from the remaining quantities. We obtain two sets of equations, one that models $P - S_v$ wave propagation and one that models S_h wave propagation. Mathematically the separation of P–S_v waves from S_h waves is an eigenvalue decomposition of the Christoffel equation, see Dellinger and Muir (1985a). For 2-D modeling of P–S_v waves, a line source perpendicular to the x, z plane with particle motion in the x, z plane is assumed; so the σ_{yy}, σ_{xy}, σ_{zy}, and e_{yy}, e_{xy}, e_{zy} terms are zero for wave propagation in the x, z plane. The 2-D $P - S_v$ stress-strain relation is

$$\begin{pmatrix} \sigma_{xx} \\ \sigma_{zz} \\ \sigma_{xz} \end{pmatrix} = \begin{pmatrix} C_{11} & C_{13} & \\ C_{13} & C_{33} & \\ & & C_{44} \end{pmatrix} \begin{pmatrix} e_{xx} \\ e_{zz} \\ e_{xz} \end{pmatrix}. \tag{6}$$

Then, by applying the law of conservation of momentum in 2-D for the in-plane stresses,

$$\begin{aligned} \frac{1}{\rho}\Big[\frac{\partial \sigma_{xx}}{\partial x} + \frac{\partial \sigma_{xz}}{\partial z} - F_x\Big] &= \frac{\partial^2 U_x}{\partial t^2} \\ \frac{1}{\rho}\Big[\frac{\partial \sigma_{zz}}{\partial z} + \frac{\partial \sigma_{xz}}{\partial x} - F_z\Big] &= \frac{\partial^2 U_z}{\partial t^2}, \end{aligned} \tag{7}$$

the particle accelerations are computed; future time levels are computed by integration.

In the axisymmetric-anisotropic case S_h waves excited by a line source perpendicular to the x, z plane with particle motion in the y direction only involve the terms $\sigma_{xy}, \sigma_{zy}, e_{xy}$, and e_{zy}. To model x, z-plane S_h wave propagation, the stress-strain relation is

$$\begin{pmatrix} \sigma_{zy} \\ \sigma_{xy} \end{pmatrix} = \begin{pmatrix} C_{44} & \\ & C_{66} \end{pmatrix} \begin{pmatrix} e_{zy} \\ e_{xy} \end{pmatrix}. \tag{8}$$

The law of conservation of momentum is,

$$\frac{1}{\rho}\Big[\frac{\partial \sigma_{xy}}{\partial x} + \frac{\partial \sigma_{zy}}{\partial z} - F_y\Big] = \frac{\partial^2 U_y}{\partial t^2}. \tag{9}$$

In both the P–S_v equations and the S_h equations, σ_{yy} and e_{yy} are zero because they only contribute to P waves propagating with a component in the cross-line direction which were ruled out by our assumption of a 2-D medium excited by a line source. A more complete treatment of axisymmetric anisotropy can be found in Dellinger and Muir (1985a).

The orthorhombic class of anisotropy, which requires nine independent elastic constants, is another convenient description of anisotropic solids. This form of anisotropy is often used to model fractured rocks, especially limestones. The orthorhombic class is the most general anisotropic model that does not couple the

normal and shear stresses, so it is the most general form that can be used on a staggered finite-difference grid without need for interpolation of stress or strain values. The stress-strain relation for a 3-D orthorhombic-anisotropic solid is given by

$$\begin{pmatrix} \sigma_{xx} \\ \sigma_{yy} \\ \sigma_{zz} \\ \sigma_{zy} \\ \sigma_{xz} \\ \sigma_{xy} \end{pmatrix} = \begin{pmatrix} C_{11} & C_{12} & C_{13} & & & \\ C_{12} & C_{22} & C_{23} & & & \\ C_{13} & C_{23} & C_{33} & & & \\ & & & C_{44} & & \\ & & & & C_{55} & \\ & & & & & C_{66} \end{pmatrix} \begin{pmatrix} e_{xx} \\ e_{yy} \\ e_{zz} \\ e_{zy} \\ e_{xz} \\ e_{xy} \end{pmatrix}. \tag{10}$$

Elastic wave field computations in an orthorhombic-anisotropic medium are usually carried out in 3-D.

FINITE-DIFFERENCE METHOD

The standard finite-difference method (Kelly et al., 1976) applied to the elastic wave equation is inadequate for large scale elastic wave field computations for two reasons. First, the use of non-centered derivatives leads to instability and inaccuracy especially for models with heterogeneous solid and liquid layers. Second, the low accuracy of the first-order finite-difference approximations to the spatial derivatives forces heavy oversampling of the spatial axes to avoid grid dispersion. When using the second-order finite-difference representation of the elastic wave equation, it is necessary to have greater than ten sample points per highest wavelength to avoid numerical dispersion and numerical anisotropy (Sword, 1987), (Marfurt, 1984). To overcome the need for oversampling, derivatives could be taken in the Fourier domain (Kosloff et al., 1984). 2-D or 3-D finite-difference algorithms that use convolutional operators and a staggered grid overcome the limitations of the standard finite-difference method as well; see Mora, (1986a) for the 2-D isotropic elastic case. As described by Mora, convolutional derivative operators can be obtained by inverse transforming the perfect operator, ik_x, truncating the result to the desired length and weighting with a gaussian taper. One advantage of a finite-difference method over the Fourier method for 3-D calculations is the ability perform multiple time steps during a single pass through the computational volume. Moreover, the finite-difference method does not need to access the variables in transposed order as does the Fourier method. For large 3-D problems accessing the data in transposed order leads to great i/o expense. Unless the entire computational volume can be held in-core or on a very fast peripheral storage device (as in (Kosloff et al., 1985)), the Fourier method is inefficient. The finite-difference method detailed here is valid for both 2-D and 3-D anisotropic elastic media including liquid layers. The staggered grid is based on that of (Mora, 1986a) and I used Mora's method for deriving accurate derivative operators.

Staggered finite-difference grid

A staggered can be used for elastic wave equation computations using centered finite-difference derivative operators. To understand the reason for using a staggered grid I will first examine the difficulty with the standard finite-difference approximation to the elastic wave equation. The standard finite-difference method would evaluate all particle displacements at the same location. For example, in the 2-D case both U_x and U_z would be known at the given grid points (x, z). When calculating the shear strain,

$$e_{xz} = \frac{1}{2}\left(\frac{\partial U_x}{\partial z} + \frac{\partial U_z}{\partial x}\right),$$

the z derivative will be centered halfway between grid points in z and the x derivative will be centered halfway between grid points in x. Since the two partials are not evaluated at the same point, it is difficult to calculate the shear strain and the shear stress. Interpolation or shifting is necessary, or inaccurate and unstable one-sided derivatives must be used. The normal strains,

$$e_{xx} = \frac{\partial U_x}{\partial x}\ ,\ e_{zz} = \frac{\partial U_z}{\partial z}$$

also are not evaluated at the same location. Calculation of normal stresses also requires shifting or interpolation.

This difficulty can be avoided by using a staggered grid. Figure 1 shows the grid used by Mora and by the 2-D version of the algorithm presented here. The displacements U_x and U_z are denoted by squares and triangles respectively. More precisely, U_x is known at$(x - \frac{1}{2}\Delta x, z)$ and U_z is known at $(x, z - \frac{1}{2}\Delta z)$. One can exploit the shifting properties of centered first derivative operators by evaluating σ_{xx} and σ_{zz} at (x, z) and σ_{xz} at $(x - \frac{1}{2}\Delta x, z - \frac{1}{2}\Delta z)$. The first step of the finite-difference algorithm for a given time step is the computation of strains and stresses from the displacements (equations 1 and 6). The derivatives

$$\frac{\partial U_x}{\partial x}\ ,\ \frac{\partial U_z}{\partial z}$$

are designed to shift forward one-half grid points, and the derivatives

$$\frac{\partial U_x}{\partial z}\ ,\ \frac{\partial U_z}{\partial x}$$

are designed to shift back one-half grid point in the direction the derivative is taken. In all cases, the spatial derivatives are taken by convolving with the derivative operators discussed above. The strains e_{xx} and e_{zz} will be evaluated at (x, z) and the shear strain e_{xz} will be evaluated at $(x - \frac{1}{2}\Delta x, z - \frac{1}{2}\Delta z)$. The elastic constants C_{11}, C_{33}, and C_{13} are assumed to be known at the points (x, z), so the stresses σ_{xx} and σ_{zz} are evaluated at the points (x, z). The elastic constant C_{44}, is known at the point $(x - \frac{1}{2}\Delta x, z - \frac{1}{2}\Delta z)$, so the shear stress σ_{xz} is evaluated at the same point.

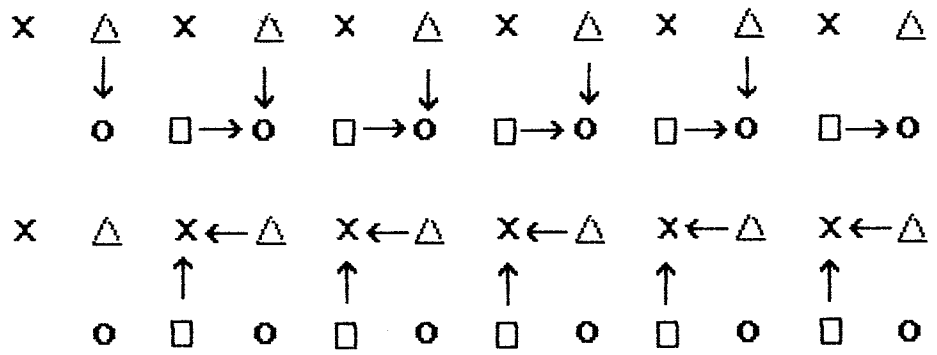

FIG. 1. Staggered grid for 2-D elastic wave field calculations. The circles are the locations of normal stresses σ_{xx}, σ_{zz}, the x's are the location of the shear stress σ_{xz}. Triangles and squares denote $\dot{U}_z$ and $\dot{U}_x$ respectively. Arrows denote spatial differentiation, and show how the derivative operators shift forward or back to compute stresses.

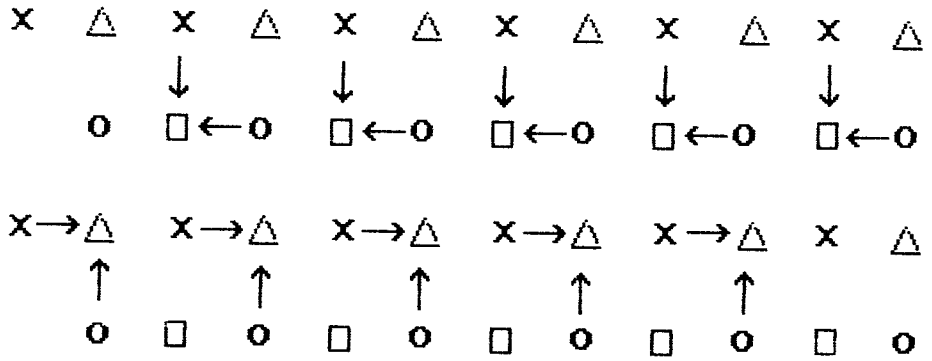

FIG. 2. Staggered grid for 2-D elastic wave field calculations. The circles denote σ_{xx} and σ_{zz}, the x's denote σ_{xz}. The triangles and squares denote $\ddot{U}_z$ and $\ddot{U}_x$ respectively. The arrows show how the derivative operators shift forward or back to compute particle accelerations from stresses.

The second step of the algorithm is the computations of particle accelerations from stresses (equation 7). For this step, the derivatives,

$$\frac{\partial \sigma_{xx}}{\partial x} \ , \ \frac{\partial \sigma_{zz}}{\partial z}$$

shift back one-half grid point in x and z respectively. The derivatives,

$$\frac{\partial \sigma_{xz}}{\partial x} \ , \ \frac{\partial \sigma_{xz}}{\partial z}$$

shift forward one-half grid point in x and z directions respectively. After this step, the spatial derivatives required for the application of the law of conservation of momentum (equation 7) are evaluated as follows:

$$\frac{\partial \sigma_{xx}}{\partial x}(x - \frac{1}{2}\Delta x, z) \ , \ \frac{\partial \sigma_{xz}}{\partial z}(x - \frac{1}{2}\Delta x, z)$$

$$\frac{\partial \sigma_{zz}}{\partial z}(x, z - \frac{1}{2}\Delta z) \ , \ \frac{\partial \sigma_{xz}}{\partial x}(x, z - \frac{1}{2}\Delta z).$$

Figure 2 shows how the derivatives are arranged to shift from stresses to accelerations. The accelerations are evaluated at the original locations of the particle displacements.

For 2-D S_h wave propagation, the particle displacement is known at the grid point (x, z), and the shear stresses σ_{xy} and σ_{zy} are known at $(x - \frac{1}{2}\Delta x, z)$ and $(x, z - \frac{1}{2}\Delta z)$ respectively. For the calculations of stresses from displacements, operators that shift back one-half grid point in x and z are applied to $U_y(x, z)$ as follows:

$$\frac{\partial U_y}{\partial x}(x - \frac{1}{2}\Delta x, z) \ , \ \frac{\partial U_y}{\partial z}(x, z - \frac{1}{2}\Delta z)$$

Strains are computed using equation (1); stresses σ_{xy} and σ_{zy} are computed using the stress-strain relation of equation (8). Then, the particle accelerations are computed using equation (9). The derivatives,

$$\frac{\partial \sigma_{xy}}{\partial x} \ , \ \frac{\partial \sigma_{zy}}{\partial z}$$

are designed to shift forward in x and z respectively, which returns the particle accelerations the values to (x, z).

The three-dimensional staggered grid is a simple generalization of the grid used for two-dimensional calculations. The 2-D grid is used on each face of the cube between (x, y, z) and $(x + \Delta x, y + \Delta y, z + \Delta z)$. The particle displacements are evaluated as follows:

$$U_x(x - \frac{1}{2}\Delta x, y, z) \ , \ U_y(x, y - \frac{1}{2}\Delta y, z) \ , \ U_z(x, y, z - \frac{1}{2}\Delta z).$$

The strains and stresses are computed from derivative operators possessing the

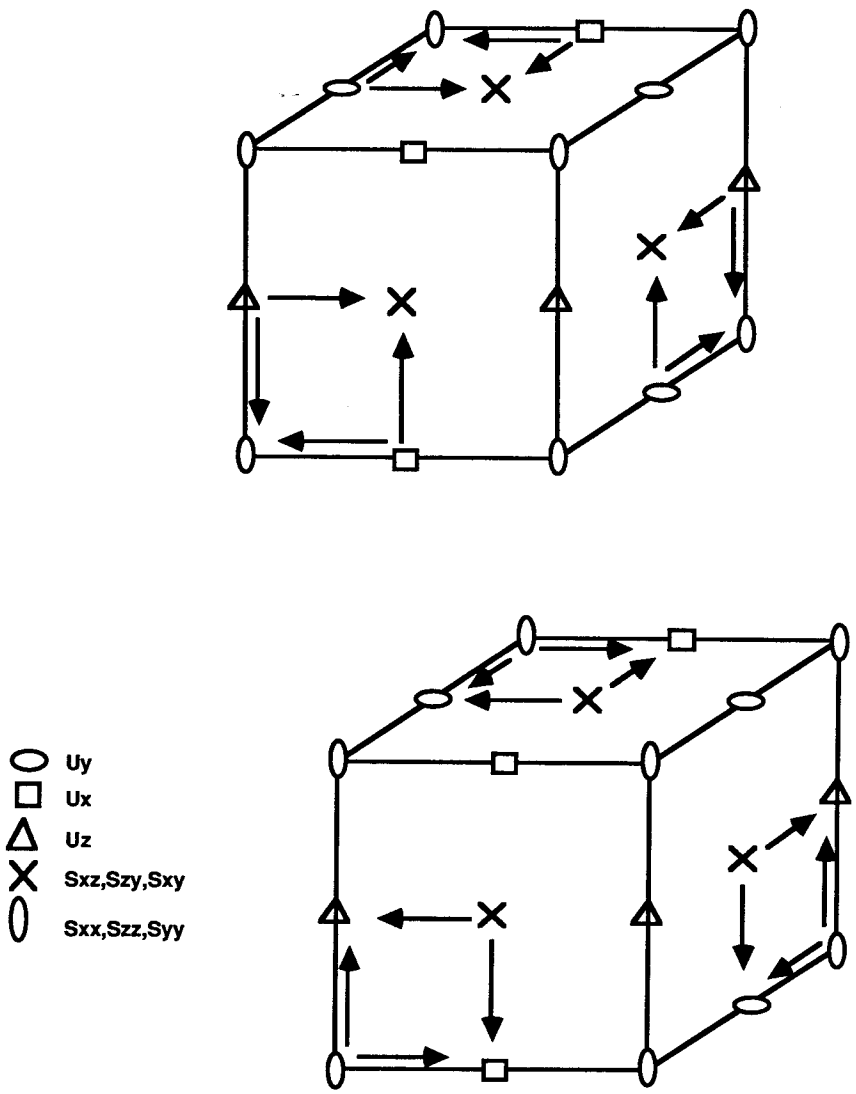

FIG. 3. Staggered grid representation for 3-D elastic wave field calculations. The top cube shows how stresses are computed from particle displacements. The bottom cube shows how particle accelerations are computed from stresses. The arrows denote spatial differentiation and show which way the derivative shifts.

same shifting properties as in the 2-D case. The stresses are then evaluated as follows:

$$\sigma_{xx}(x,y,z)\ ,\ \sigma_{yy}(x,y,z)\ ,\ \sigma_{zz}(x,y,z),$$

and

$$\sigma_{zy}(x,y-\frac{1}{2}\Delta y,z-\frac{1}{2}\Delta z)\ ,\ \sigma_{xz}(x-\frac{1}{2}\Delta x,y,z-\frac{1}{2}\Delta z),$$

$$\sigma_{xy}(x-\frac{1}{2}\Delta x,y-\frac{1}{2}\Delta y,z).$$

Using the same principles as in the 2-D case, the derivatives taken to find the particle accelerations shift forward or back as needed. The top cube of Figure 3 shows how stresses are computed from the particle displacements; the bottom cube shows how particle accelerations are computed from stresses. As above, all spatial derivatives are taken by finite-differences using the convolutional operators of Mora.

Boundary conditions

To reduce unwanted reflections from the sides and bottom of the computational grid, an elastic version of the B1 boundary condition described by Clayton and Engquist (1977) is incorporated into the 2-D and 3-D algorithms. The boundary conditions are designed to absorb horizontally propagating plane waves striking the side boundaries and vertically propagating plane waves striking the bottom boundary (Vidale and Clayton, 1986). For 2-D and 3-D propagation, equations similar to equations 8 and 9 of Vidale and Clayton are used with velocities modified to absorb anisotropic waves. The greatest advantage of the B1 conditions that they require no extra storage and very few computations. The "sponge" type absorbing boundaries described by Cerjan et al. (1985) are not useful for 3-D computations because they require many points to be effective, and the full elastic equation still has to be solved in the boundaries.

The free surface at the top of the grid is modeled by forcing normal and tangential stresses to be zero at the top of the grid. It is not possible to put both the shear stresses σ_{xz} and the normal stress σ_{zz} (in the 2-D case) on the surface because of the staggered grid. I chose to place σ_{xz} on the surface; it is explicitly forced to be zero at the top of the grid. Since σ_{zz} is not known at the surface, but at one-half grid point above and below the free surface, the vertical derivative of σ_{zz} must be modified when computing the vertical particle acceleration at the free surface. This modification is tantamount to forcing σ_{zz} to be zero at the free surface by interpolation.

Many details of the implementation of the finite-difference method depend on computer architecture and will not be discussed at length. However, it is important to describe one aspect of the implementation of the finite-difference method for 3-D models. For many 3-D models, the volume of computational variables cannot be held in the core memory of even the largest computers. It is necessary to consider how the algorithm can handle the storage and retrieval of intermediate

results from a disk or other storage device. If the data are organized as a set of constant y planes, the necessary computations to update a given plane to the next time level only requires the information from nearby planes. For example, if eight point convolutional derivative operators are used, then the calculation of stresses from displacements involves eight planes. Similarly, the calculation of particle accelerations from stresses would also involve eight planes. Stew Levin (pers. comm.) suggested equating one time step of the elastic wave equation with applying an operator to the computational volume. The operator contains the spatial derivatives for calculation of stresses, accelerations, and the time integration calculations. One time step of the algorithm involves sweeping through the computational volume as a sequence of planes applying the operator to update the entire volume one time step. The operator is spatially compact because the spatial differentiation operators only extend a "few" points in each direction. The volume has to be read and written only once for each time step. Moreover, the data do not have to be accessed from disk in transposed order. To further reduce the cost of i/o, the algorithm can perform the computations for two or more time steps on one pass through the computational volume by cascading the operator for one time step, forming a multistep operator. Then the volume has to be read and written only once for every two or more time steps.

RESULTS

Modeling

The finite-difference method presented here can compute the elastic wave field in a heterogeneous anisotropic model due to a variety of sources. However, it is worthwhile to examine the method in a simple case. The solution to the elastic wave equation in a homogeneous half-space with a source at the free surface, known as Lamb's problem, is well known and serves as a reference point for numerical wave propagation algorithms. Figure 4 shows snapshots of vertical and horizontal particle acceleration of the P–S_v wave field in a homogeneous medium excited by a vertical force at the free surface at the top of the model. The P, S_v, and $P-S_v$ head waves are modeled and the Rayleigh wave at the free surface propagates without dispersion. Figure 5 shows horizontal and vertical particle acceleration seismograms observed at the free surface. Again notice that the wave types are correctly propagated, especially the Rayleigh wave. Figure 6 shows snapshots of the S_h wave response to Lamb's problem.

The finite-difference method explained here was designed for elastic media, but can be used without modification to propagate waves through a combination of solid and liquid layers. Figure 7 shows snapshots of the vertical and horizontal particle accelerations of the wave field in a liquid layer over a homogeneous anisotropic solid layer. Note the P–S_v conversions and head waves occurring at the boundary between the solid and liquid media.

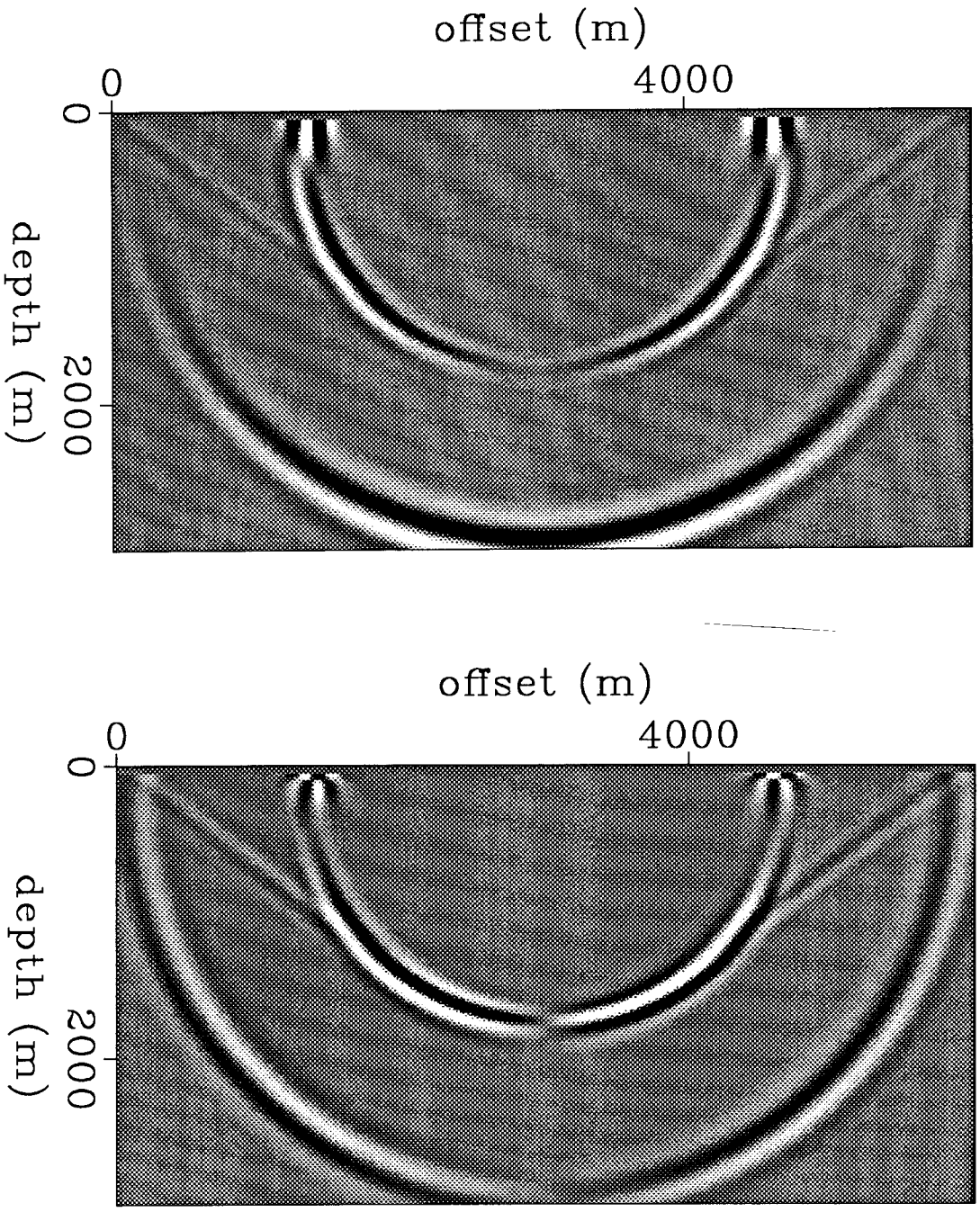

FIG. 4. Snapshots showing vertical and horizontal components of particle acceleration for solution to Lamb's problem in 2-D. Note the Rayleigh wave on the free surface that propagates without dispersion. The source time history was a second-derivative gaussian pulse with 15 Hz center frequency.

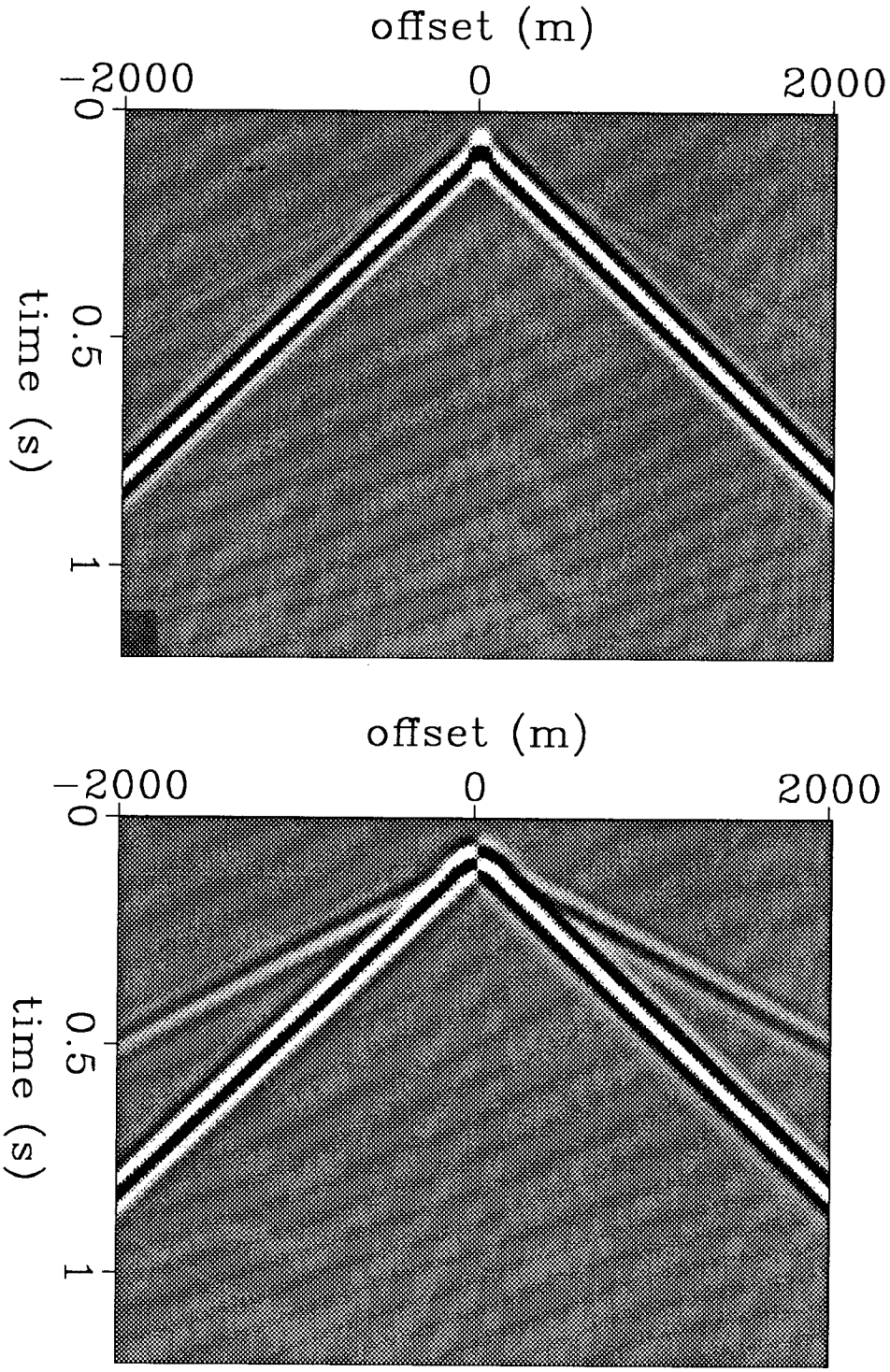

FIG. 5. Vertical and horizontal components of particle acceleration at surface. Solution to Lamb's problem in 2-D. The Rayleigh wave on the free surface propagates without dispersion.

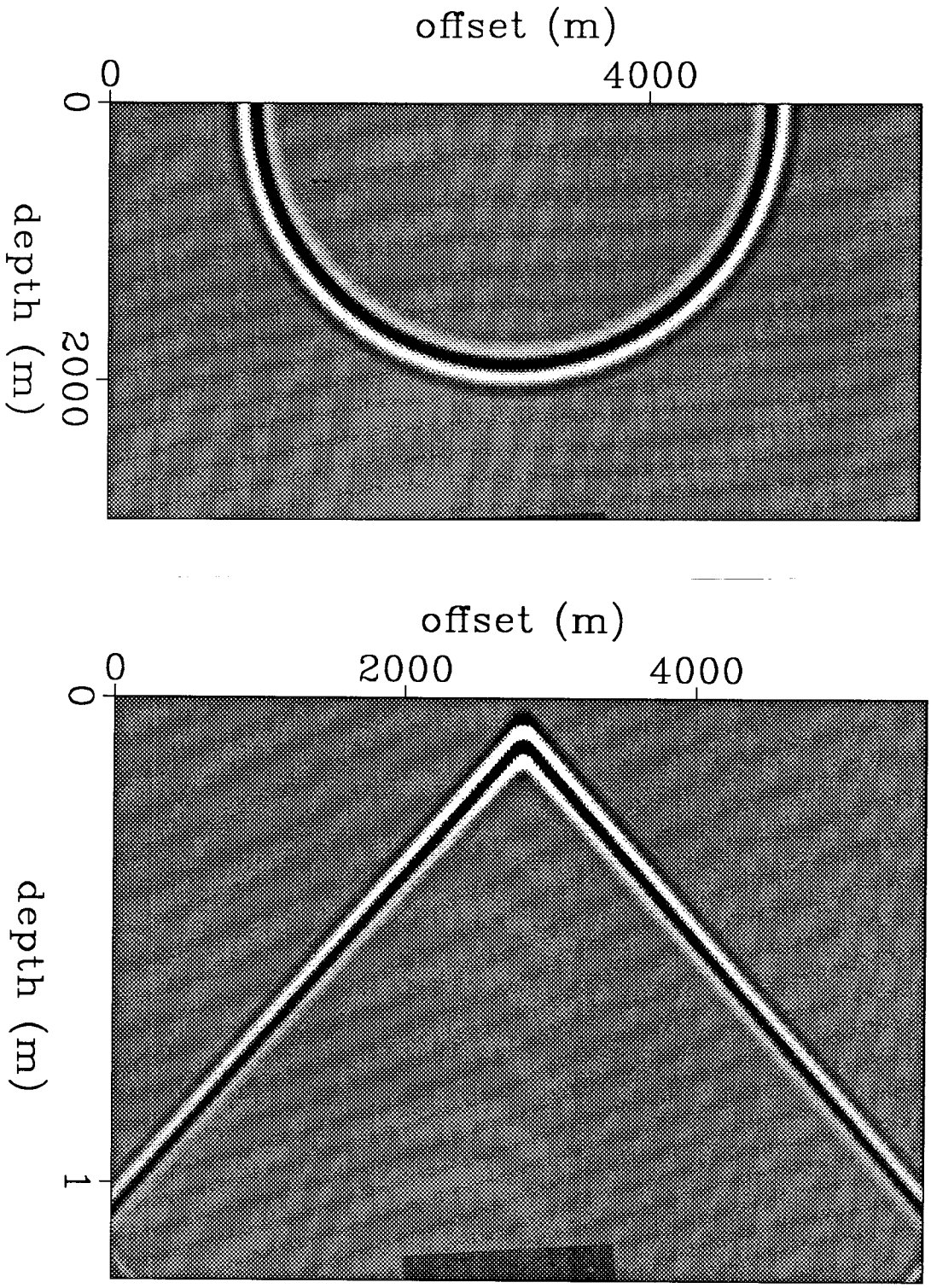

FIG. 6. Cross-line horizontal component (S_h wave) snapshot and surface seismogram. solution to Lamb's problem in 2-D computed by the S_h wave equation. In this case there is no Rayleigh wave in the x, z-plane.

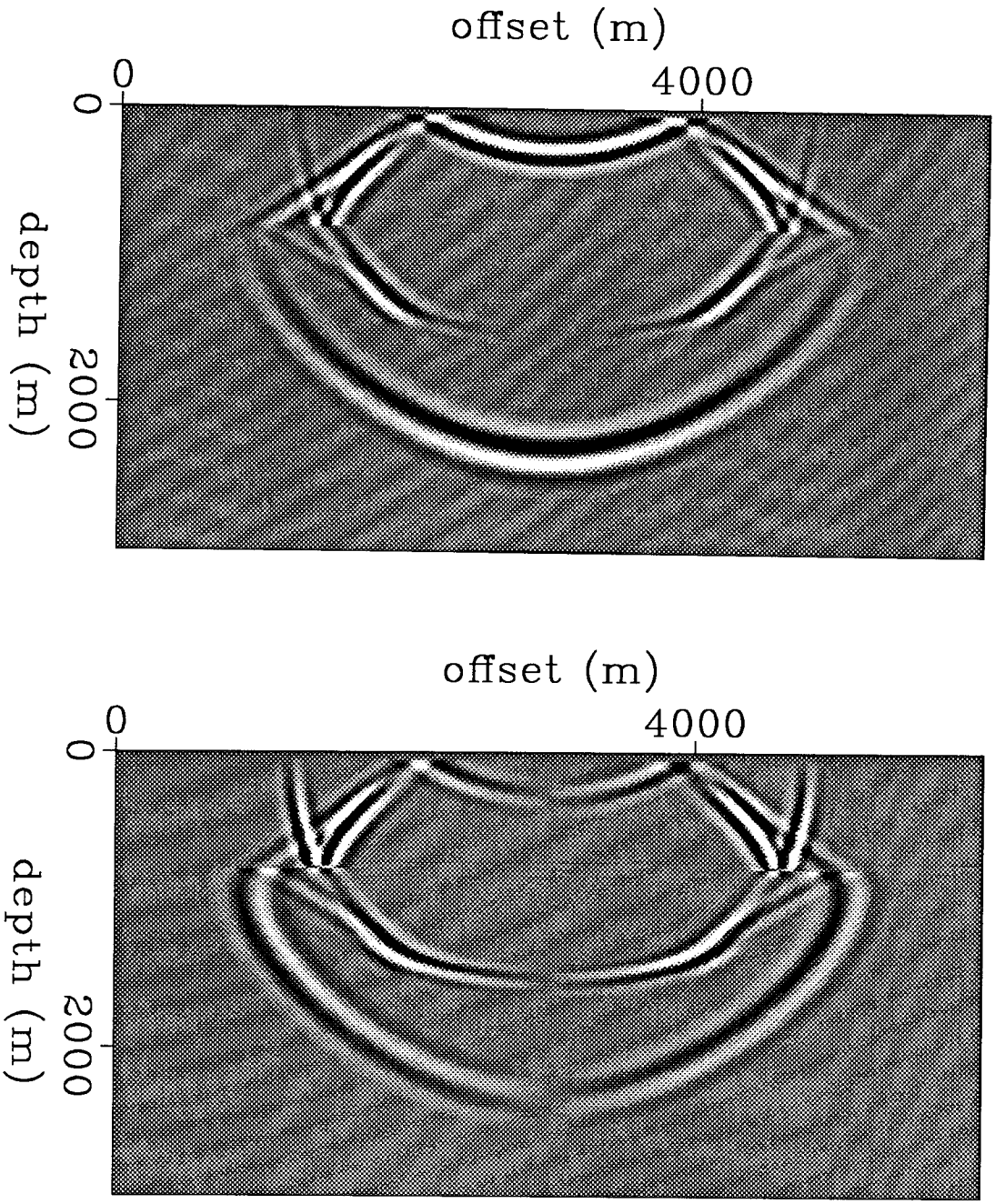

FIG. 7. Snapshots of vertical (top) and horizontal (bottom) components of particle acceleration for wave propagation in a liquid layer above an anisotropic solid layer. Wave conversion is correctly modeled at the solid-liquid interface.

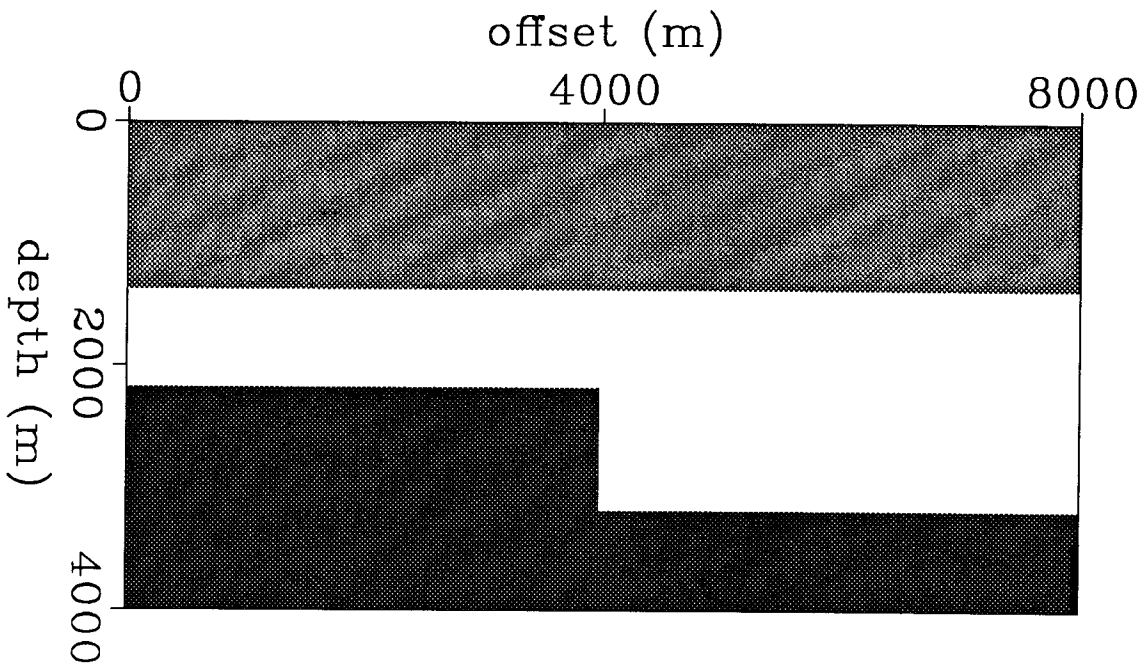

FIG. 8. Geologic model for axisymmetric-anisotropic P–S_v and S_h wave propagation. The elastic constants stay fixed within each layer, and represent the "Greenhorn shale" and other anisotropic rocks.

The elastic wave field in a complicated anisotropic model is usually not known analytically, but the performance of the algorithm can still be judged in a qualitative fashion. To model the elastic wave field in an axisymmetric-anisotropic medium, the 2-D version of the finite-difference method can be used. The geologic structure for the model consists of two anisotropic layers over a fault block. The elastic constants for the top layer were taken from the "Greenhorn shale" of Dellinger and Muir (1985a). The elastic constants for the remaining layers were derived by varying the elastic constants of Greenhorn shale. Figure 8 shows the structure of the geologic model. Figures 9 and 10 show snapshots at two time levels of the P–S_v wave field in the axisymmetric-anisotropic model due to a vertical force at the free surface. The anisotropic nature of the wave field is evident, the S_v wave triplicates, and the P wave propagates with a "football" shaped wave front. Figure 11 shows two snapshots of the S_h wave field in the same model. The S_h wave is elliptical in the top layer. The wave field behavior (both P–S_v and S_h) in the top layer qualitatively agrees with results shown by Dellinger (1985b). Figure 12 shows the cross-line horizontal component of the surface seismogram recorded for this model. Figures 13 and 14 show the in-line horizontal and vertical component seismograms for the model. The various mode-converted reflections, diffractions, and direct waves including the Rayleigh wave are present.

The elastic wave field in an orthorhombic-anisotropic heterogeneous model may be quite complex. Confidence in the method, gained through simple examples

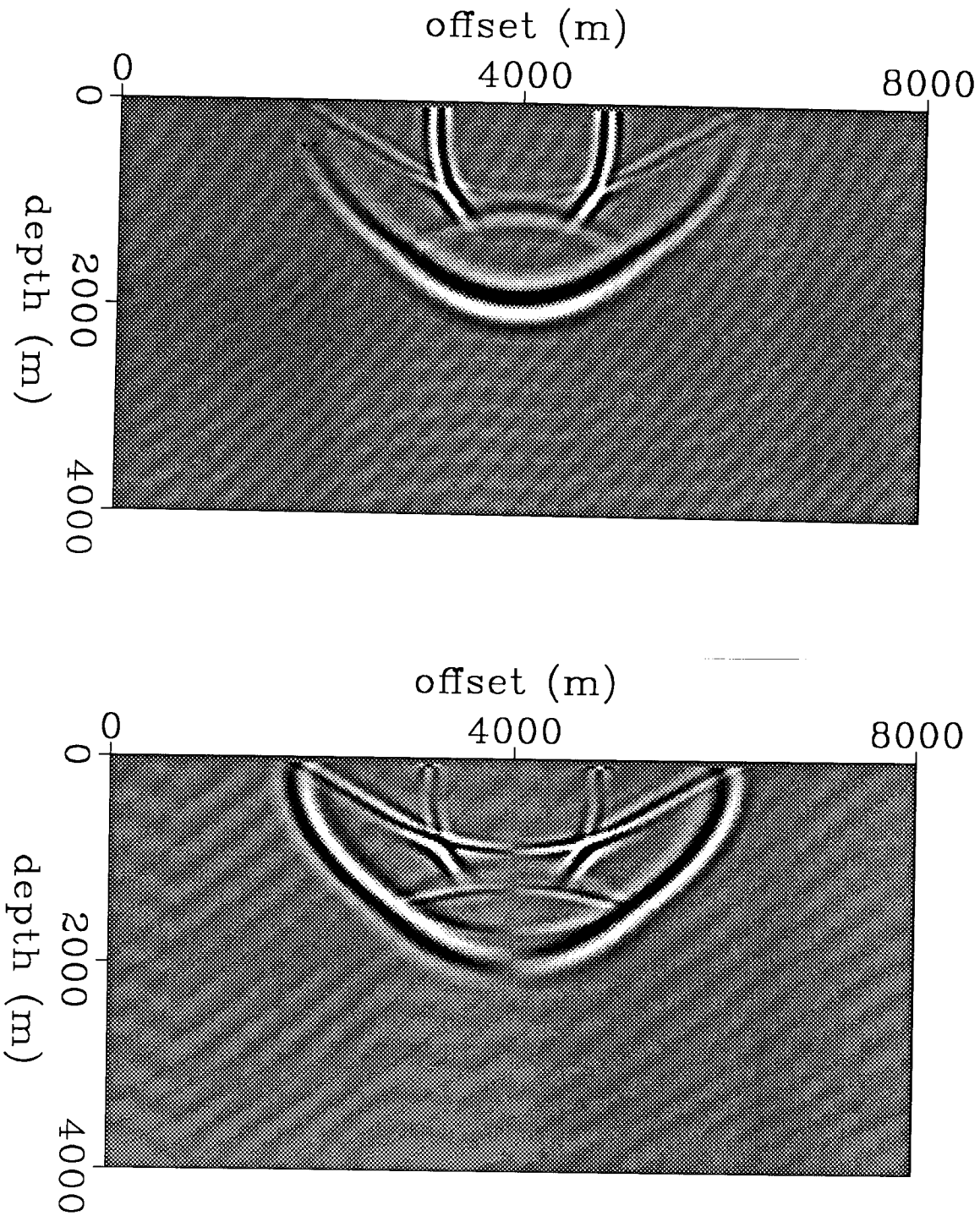

FIG. 9. Snapshots of vertical and horizontal components of particle acceleration for elastic anisotropic wave propagation in a complex model. Note P–S_v conversions, triplicating direct S_v wave and Rayleigh wave at the free surface.

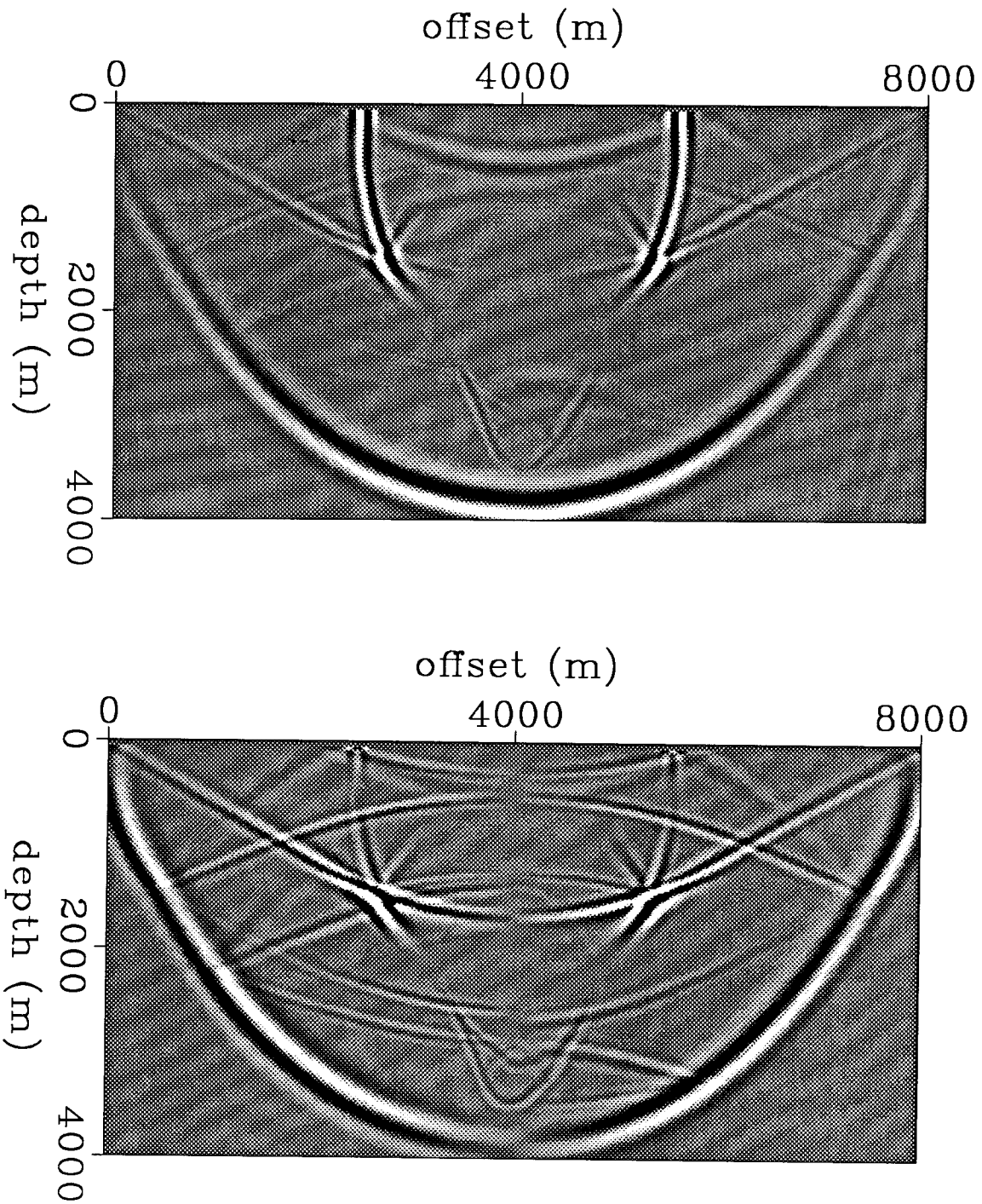

FIG. 10. Snapshots of vertical and horizontal components of particle acceleration for elastic anisotropic wave propagation in a complex model at a later time. Note P–S_v conversions, P–S_v diffractions, Rayleigh wave, and triplicating direct S_v wave, reflections from the free surface and diffractions from the fault block.

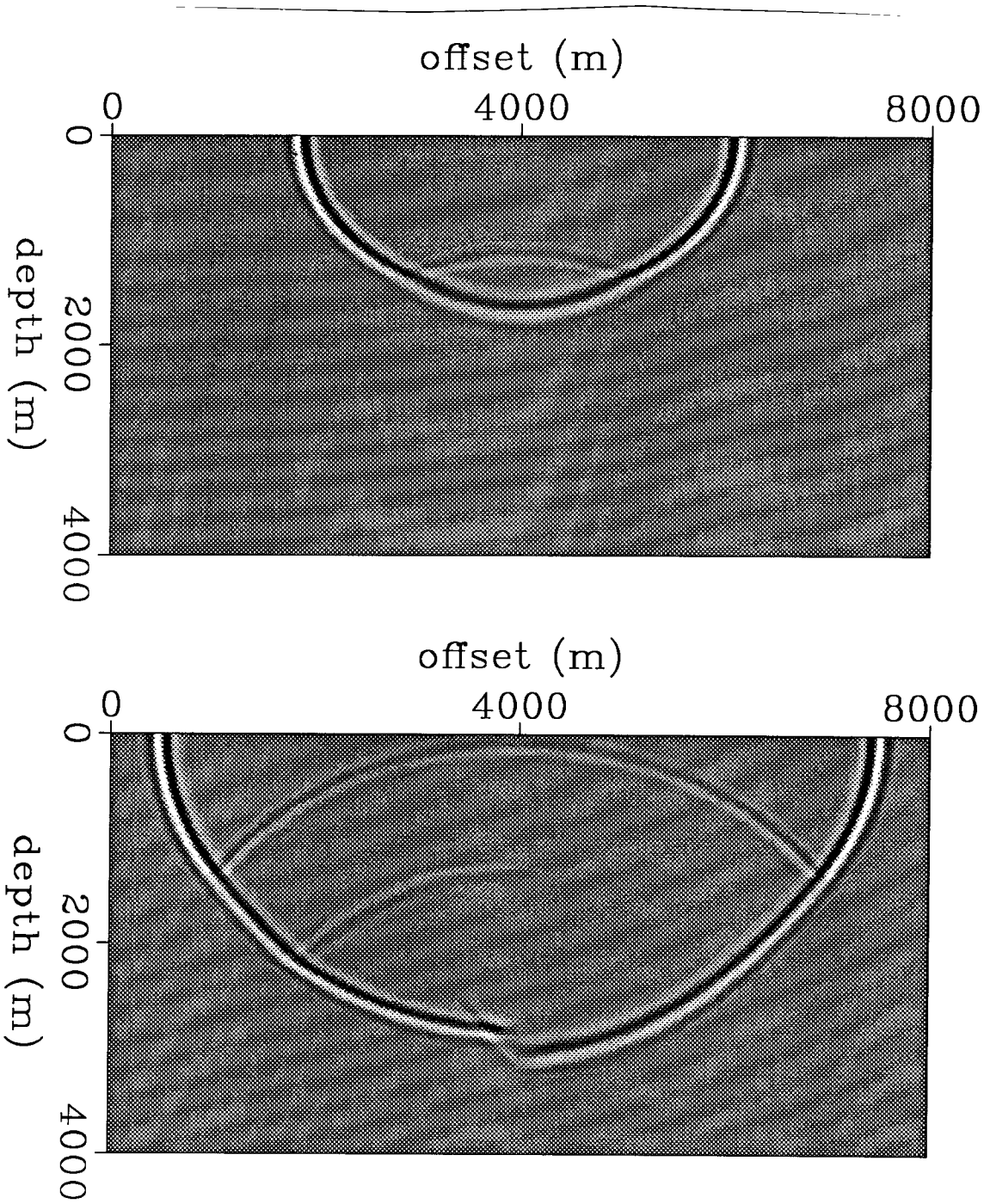

FIG. 11. Snapshots of cross-line horizontal component of particle acceleration for elastic anisotropic wave propagation in a complex model at two time levels. There is no coupling with the P–S_v wave equation since the medium is assume to have no cross-line variations and is transversely isotropic. The S_h wave has an elliptical shape as expected (Dellinger and Muir, 1985a).

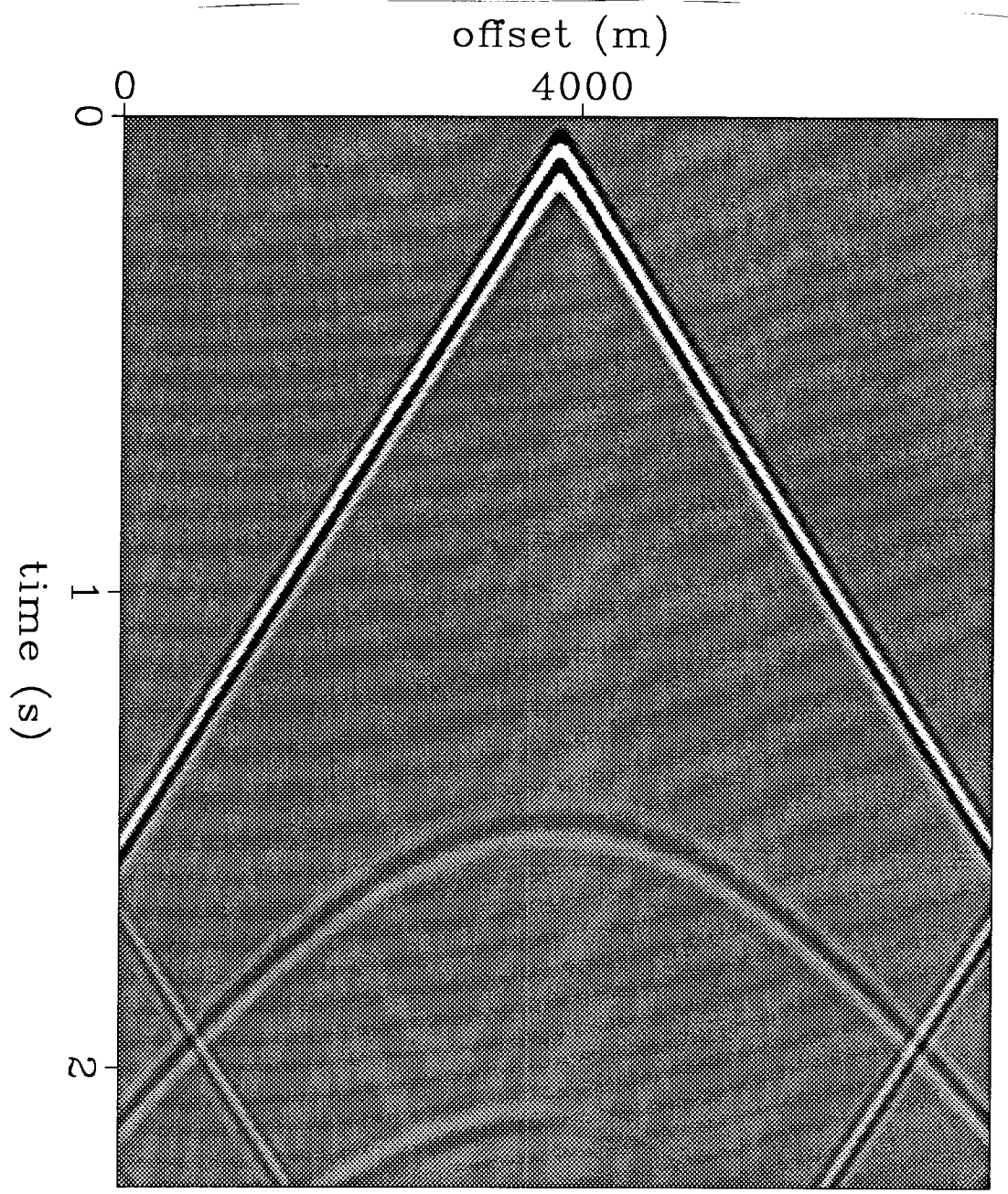

FIG. 12. Cross-line horizontal component of particle acceleration at the surface collected over heterogeneous anisotropic 2-D model. Only S_h waves are present in this section.

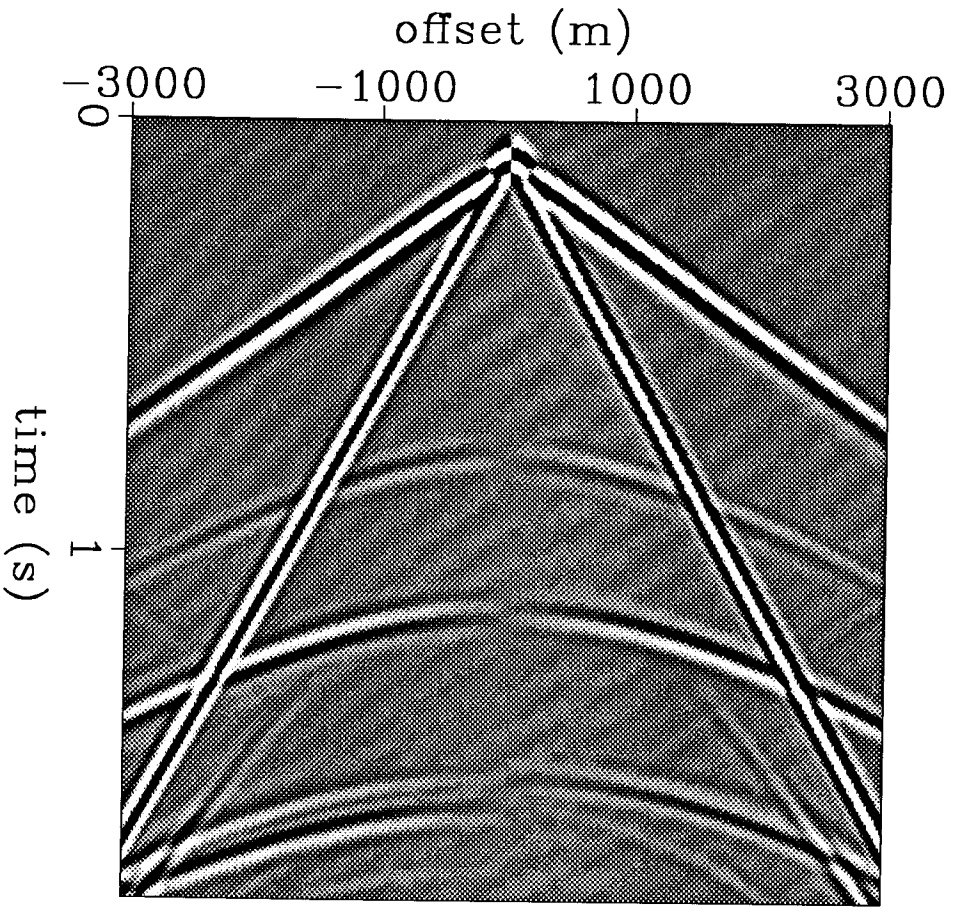

FIG. 13. In-line horizontal component of particle acceleration collected over heterogeneous anisotropic 2-D model. Note non-dispersive Rayleigh wave and various reflected and mode-converted arrivals.

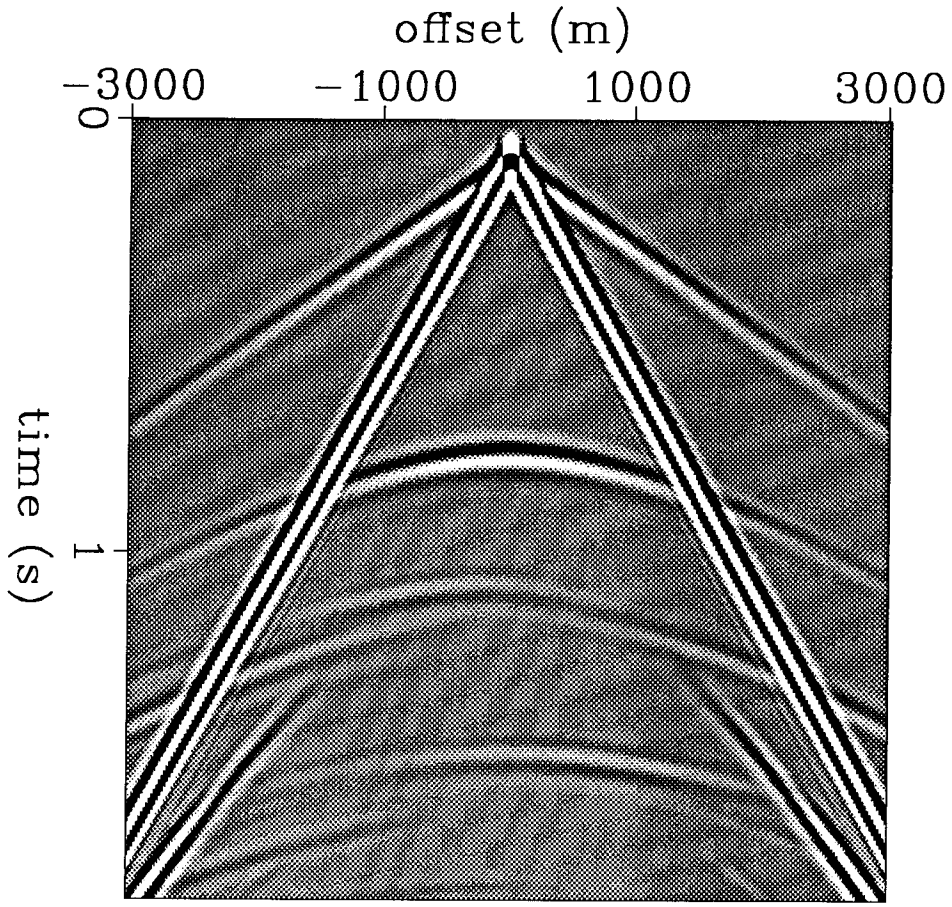

FIG. 14. Vertical component of surface seismogram collected over 2-D heterogeneous anisotropic model. Rayleigh wave present, along with several reflected and mode-converted arrivals.

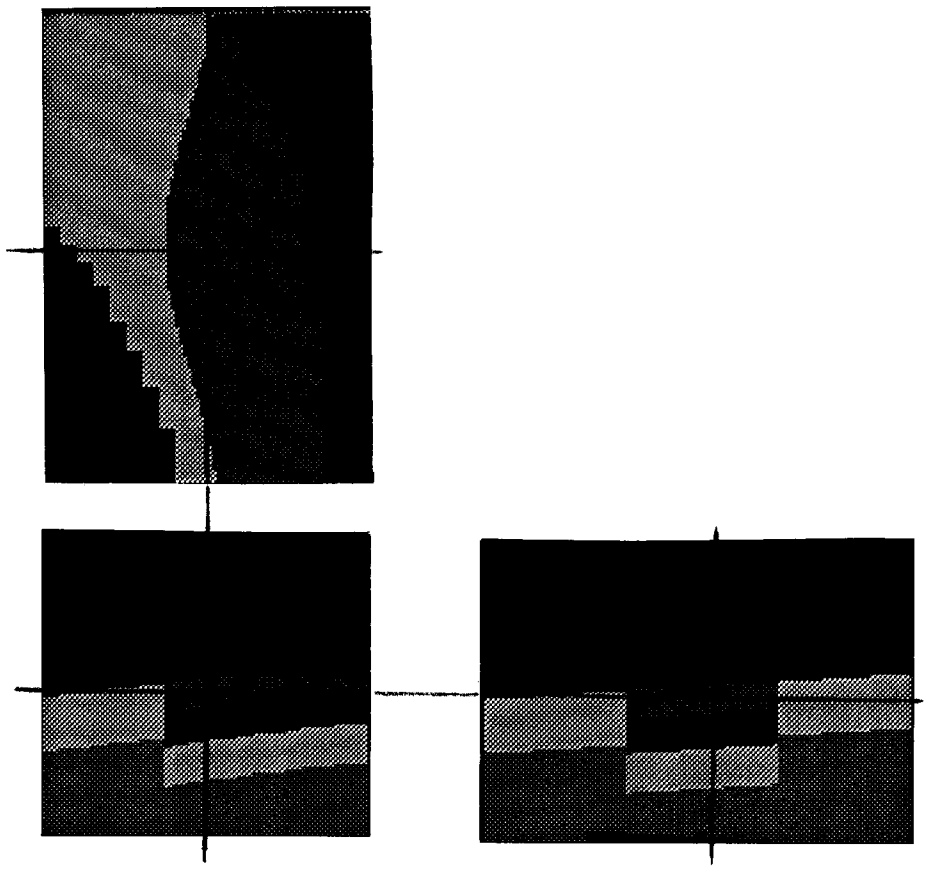

FIG. 15. Plan view of orthorhombic-anisotropic geologic model. The lighter layers represent fractured limestones. The "cracks" are in the y, z-plane.

supports the belief that the method will behave correctly in the 3-D orthorhombic anisotropic case. Figure 15 shows a plan view representation of the 3-D orthorhombic-anisotropic model used in this section. The darkest layer is the Greenhorn shale, and is axisymmetric anisotropic. The lighter layers represent fractured limestones (orthorhombic anisotropic class). P wave velocity varies by 25 percent depending on direction; S wave velocity varies by a similar amount depending on the polarization of the shear wave. Snapshots of the elastic wave field the orthorhombic-anisotropic heterogeneous 3-D model calculated by the finite-difference method of this paper is shown in Figures 16, 17, 18, 19, and 20.

The source was a force on the free surface applied to a small region with linearly polarized particle motion in the x, z plane 45 degrees from vertical. Figures 21, 22,

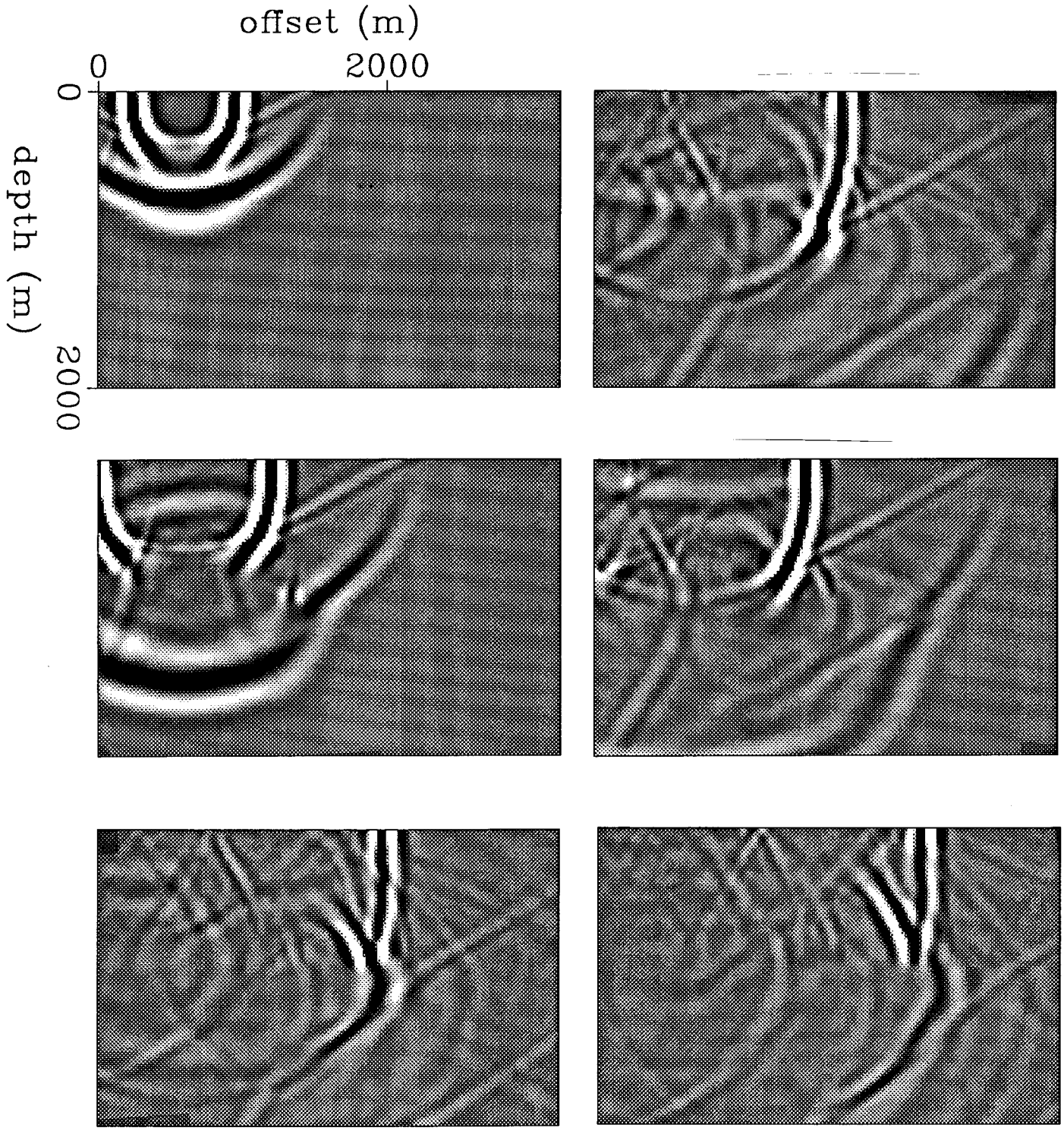

FIG. 16. Snapshots of vertical component of particle acceleration for 3-D elastic orthorhombic-anisotropic wave field. Frames are sampled every .15 seconds starting at .3 seconds. Each frame is a taken from a constant y slice through the computational model containing the source point.

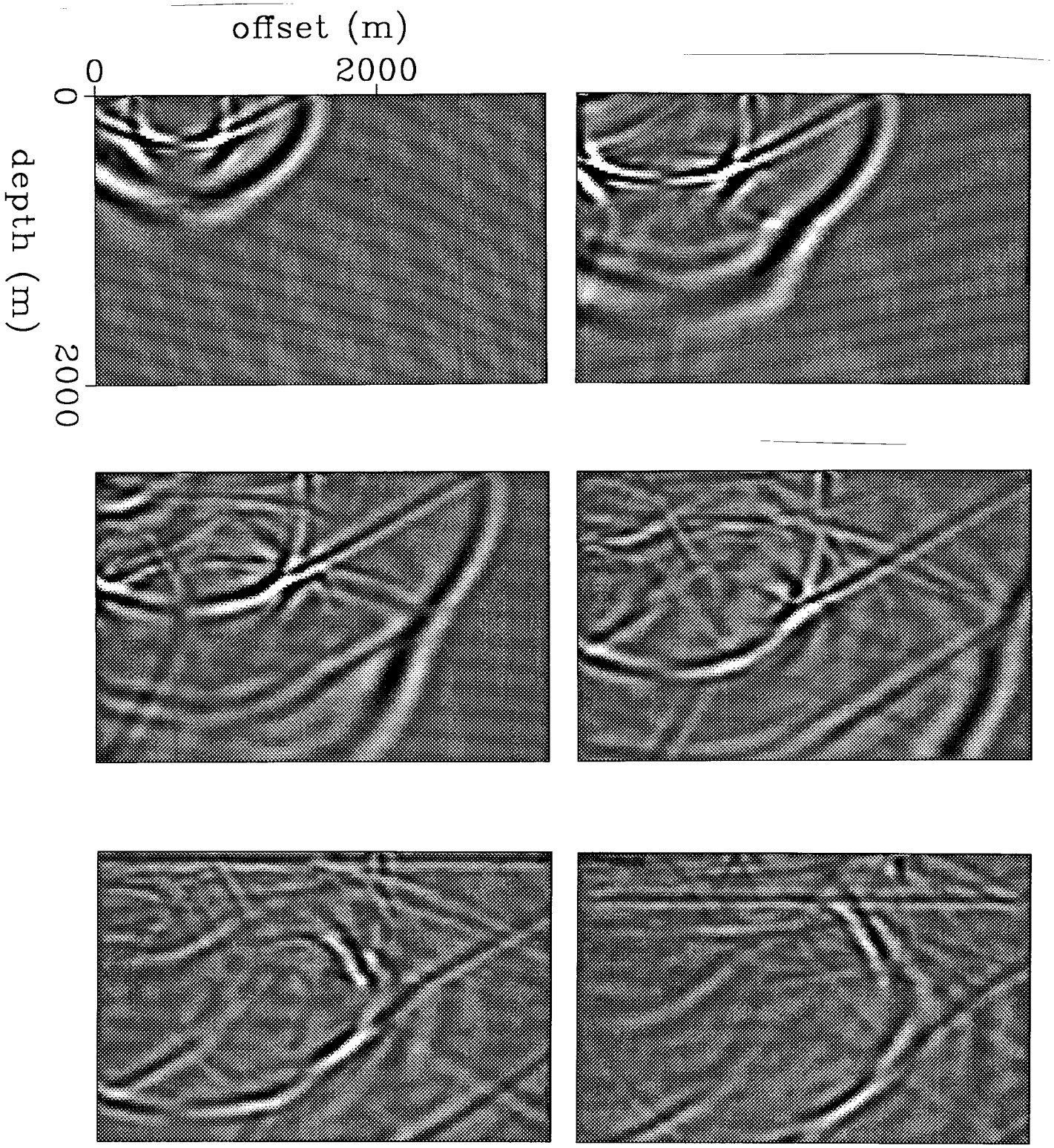

FIG. 17. Snapshots of x component of particle acceleration. The slices are at the same locations as for the vertical particle accelerations.

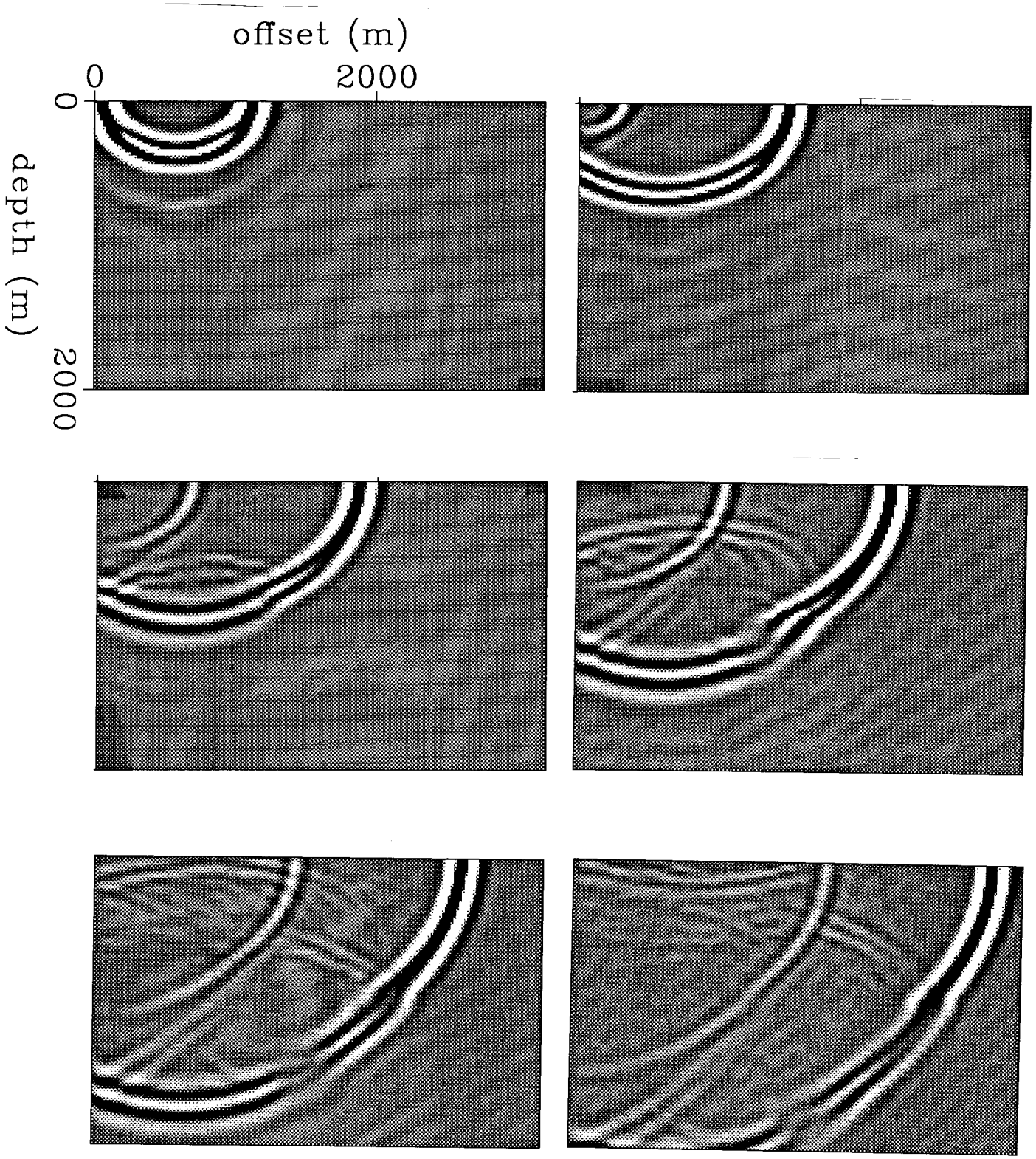

FIG. 18. Snapshots of y component of particle acceleration. Same location as previous two figures.

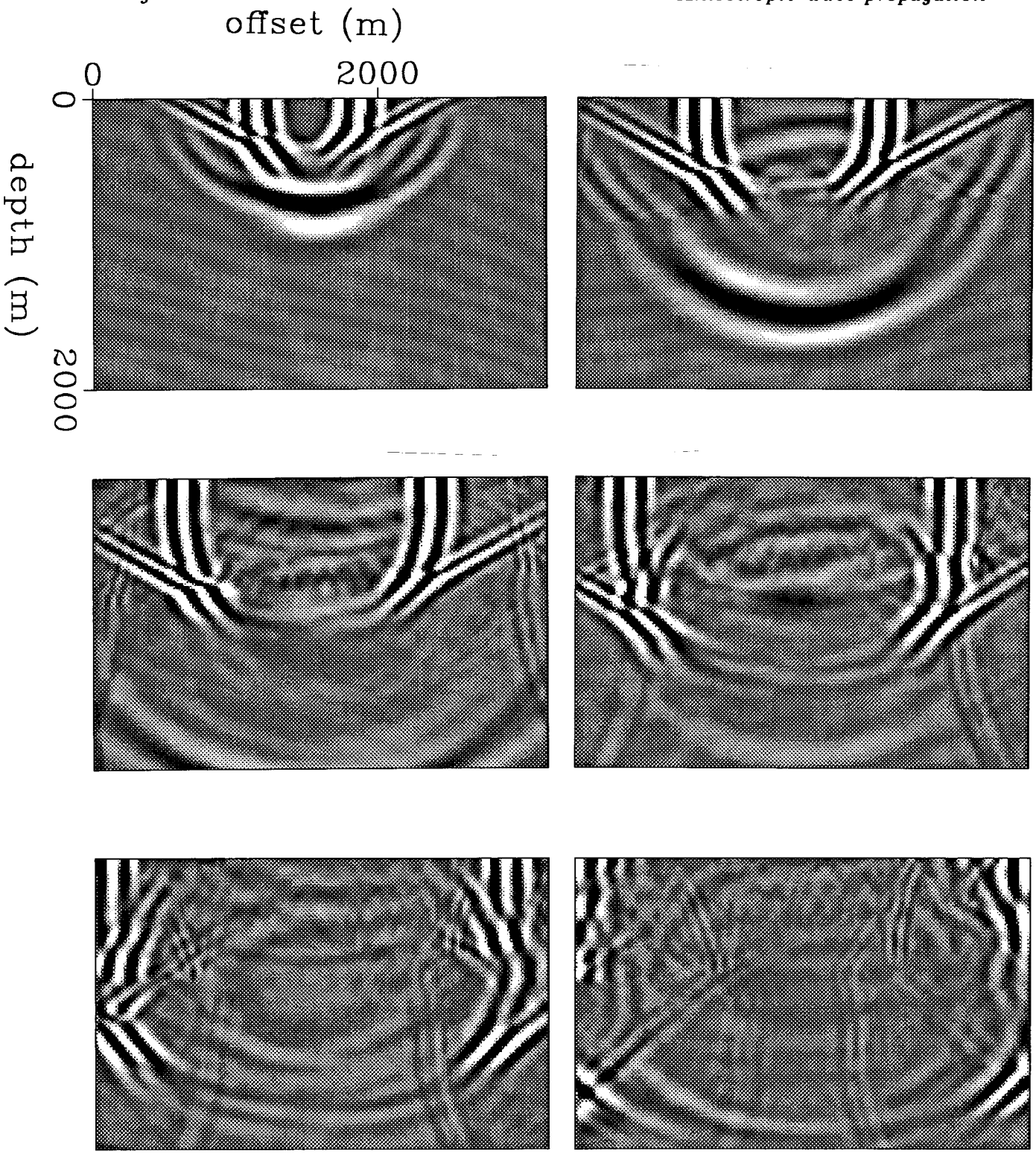

FIG. 19. Snapshots of vertical component of particle acceleration for 3-D orthorhombic-anisotropic elastic wave field. Frames are sampled every .15 seconds starting at .3 seconds. Each frame is a taken from a constant x slice through the computational model containing the source point.

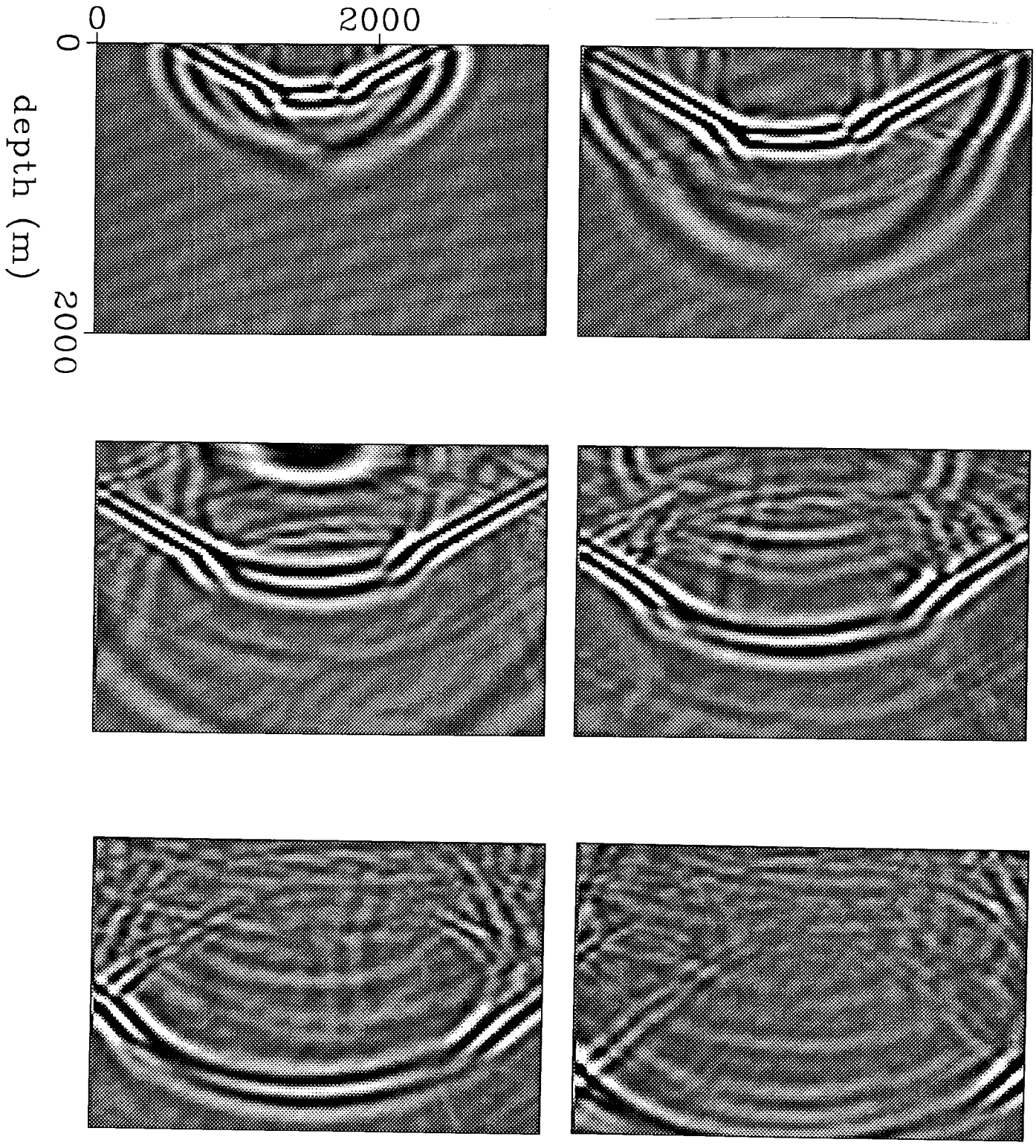

FIG. 20. Snapshots of y component of particle acceleration taken from the same location as the z component shown in the last figure.

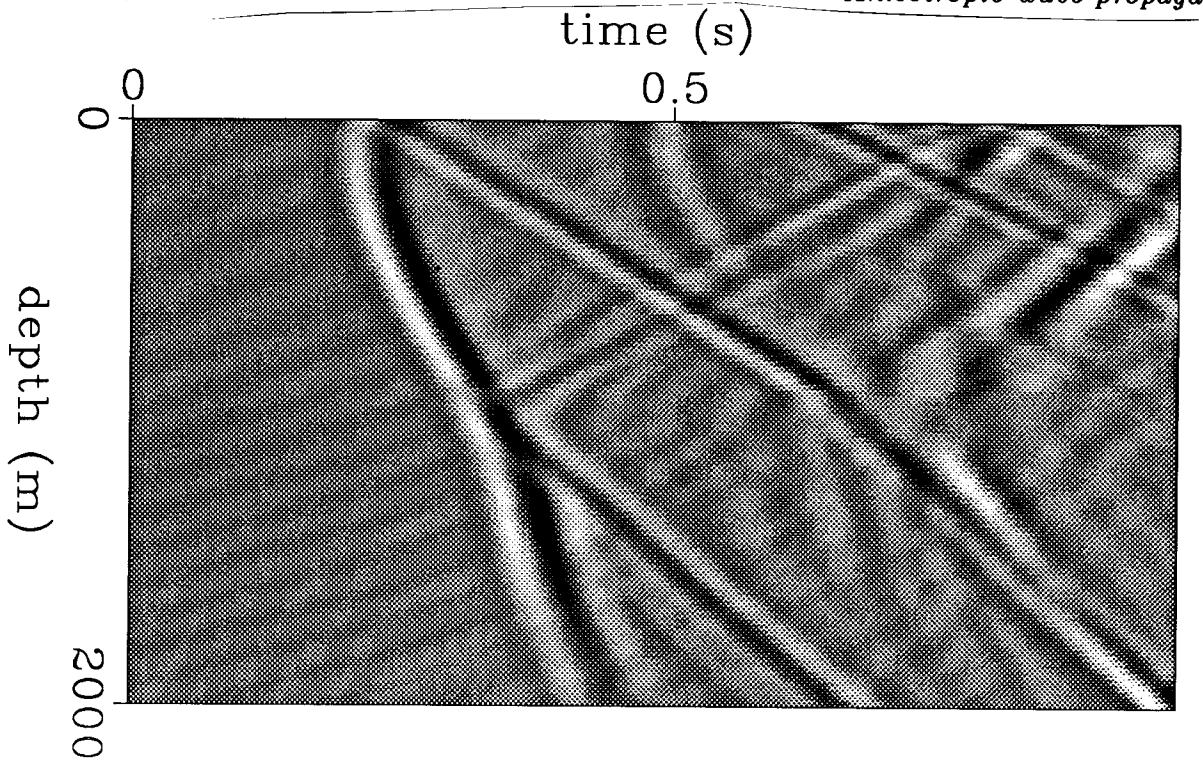

FIG. 21. X component of the VSP recorded in an orthorhombic-anisotropic 3-D model. The well was located 1 600 meters from the source location in the x direction. The source was linearly polarized at 45 degrees in the y, z-plane.

and 23 are a 3-component VSP collected at offset 1 600 meters in the x direction from the source location.

Prestack Migration

The wave propagation method of this paper is also useful for migration of elastic wave fields in anisotropic media. Prestack migration of an elastic wave field is an extension to acoustic prestack reverse time migration (see Etgen (1986) for the acoustic case and Mora (1986b) for the elastic isotropic case). The recorded wave field, in this case from an elastic anisotropic medium, is time reversed and propagated back into the subsurface model. Imaging is accomplished by correlating with the source wave field which is also propagated in reversed time. Figure 24 shows an S_h wave shot profile gathered over an axisymmetric-anisotropic elastic medium. Figure 25 shows the recorded data propagating in reversed time, and Figure 26 shows the imaged section using anisotropic wave propagation. The reflectors are imaged and positioned correctly in depth. Figure 27 shows the same data imaged using isotropic wave propagation, where the velocity was chosen to be the horizontal velocity of the medium. The image is not positioned correctly in depth and the structure is incorrect. It is also possible to image the P–S_v section using reverse-time migration, but more complicated imaging conditions beyond the scope of this paper are necessary to unscramble the coupled wave fields.

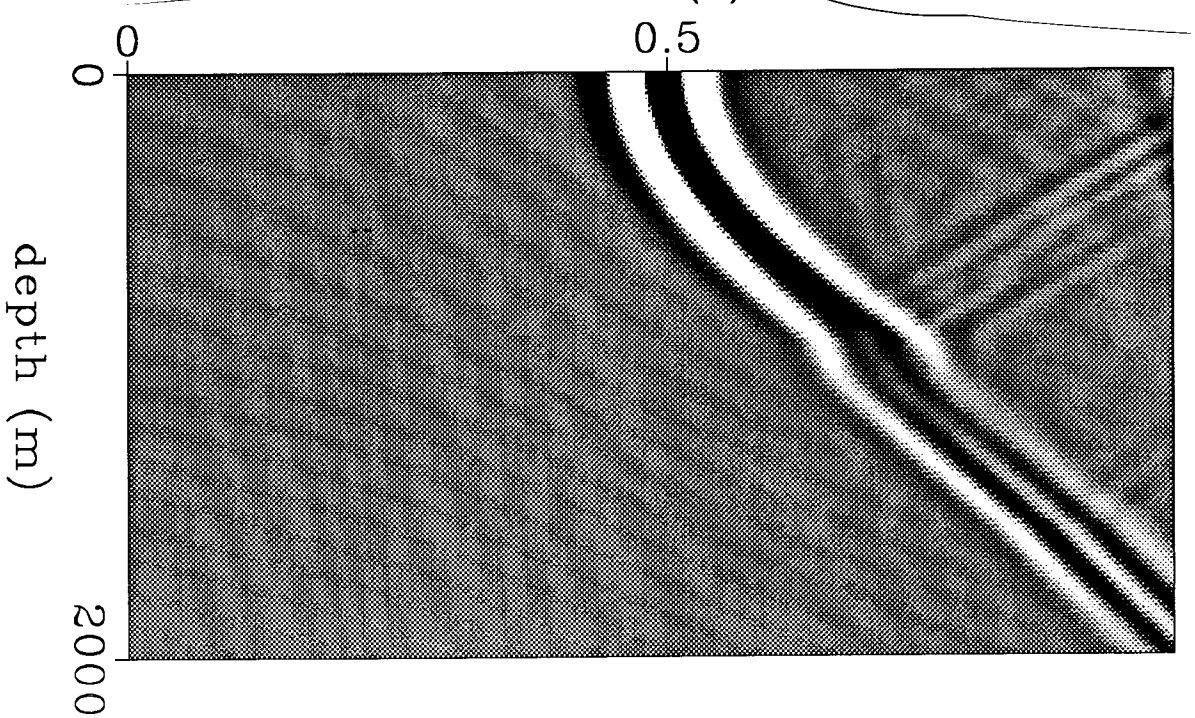

FIG. 22. Y component of the VSP in the 3-D model.

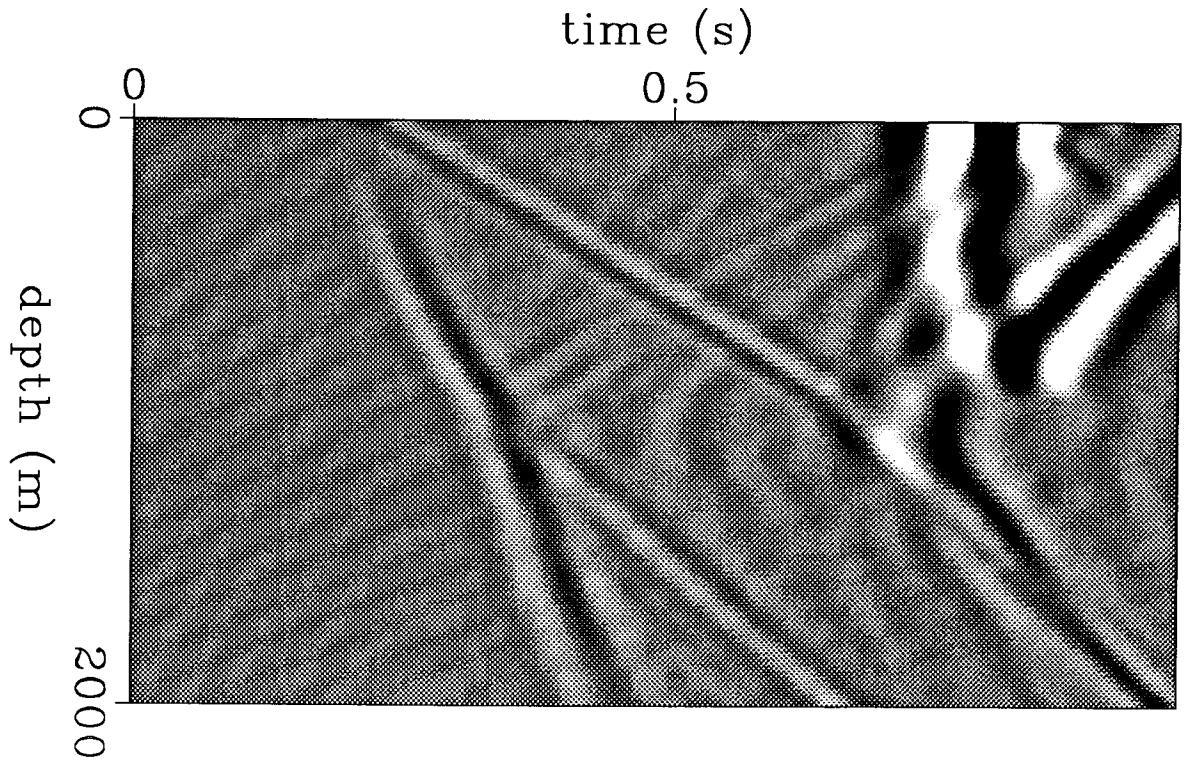

FIG. 23. Z component of the VSP in the 3-D model.

CONCLUSIONS

The elastic wave equation can be solved in heterogeneous anisotropic media using a finite-difference technique. The method computes wave fields in both 2-D and 3-D models. The 2-D version assumes an axisymmetric-anisotropic medium (with a vertical symmetry axis) with no y-direction variations excited by a line source. The resulting P–S_v equation and S_h wave equation are solved separately on 2-D grids. The 3-D version allows both axisymmetric anisotropy and orthorhombic anisotropy both with arbitrary geologic structure. A variety of outputs are produced; snapshots, surface seismograms and VSP's can be collected for a given model. The 3-D version uses an efficient out-of-core technique to reduce i/o cost and allow computation of large scale 3-D elastic models. Both the 2-D and 3-D methods produce accurate synthetic seismograms and I show how to use the S_h wave equation to image an anisotropic subsurface using reverse-time migration.

Modeling the Earth as a solid and removing the standard assumption of isotropy should lead to better understanding of wave fields that propagate in the Earth and to better methods of imaging the subsurface. The finite-difference technique presented here can be used for modeling wave fields in the subsurface and for imaging wave fields observed at the surface or in a borehole.

ACKNOWLEDGMENTS

I would like to thank Pete Mora for many discussions of finite-difference wave propagation and for showing me his staggered grid method. I also thank Joe Dellinger and Francis Muir for their many insights into anisotropic wave propagation. Finally thanks go to Stew Levin for showing me his "AP" trick to reduce i/o cost.

REFERENCES

Cerjan, C., Kosloff, D., Kosloff, R., Reshef, M., 1985, Short note: A non-reflecting boundary condition for discrete acoustic and elastic wave equations: Geophysics, **50**, 705-708.

Clayton, R. W. and Engquists, B., 1977, Absorbing boundary conditions for acoustic and elastic wave equations: Bull., Seis. Soc. Am., **67**, 1529-1540.

Dellinger, J. and Muir, F., 1985a, Axisymmetric anisotropy I: Kinematics: SEP-42, 1-25.

Dellinger, J., 1985b, Some anisotropic modeling examples: SEP-44, 63-66.

Etgen, J.T., 1986, Prestack reverse time migration of shot profiles: SEP-50, 151-169.

Kelly, K. R., Ward, R. W., Treitel, S., and Alford, R. M., 1976, Synthetic seismograms: A finite-difference approach: Geophysics, **41**, 2-27.

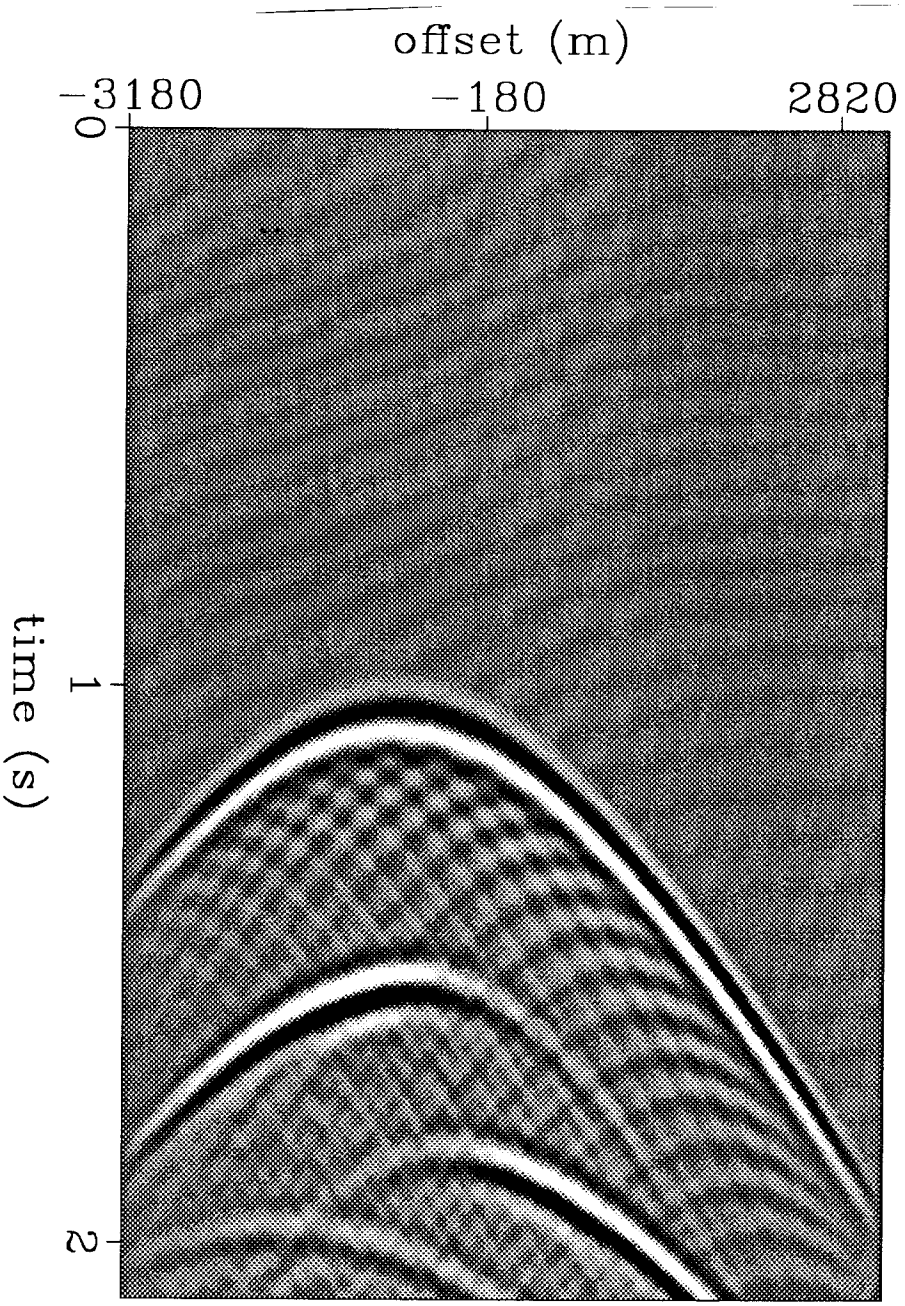

FIG. 24. Surface seismogram of cross-line particle acceleration, S_h waves, recorded over a dipping layer, fault block model.

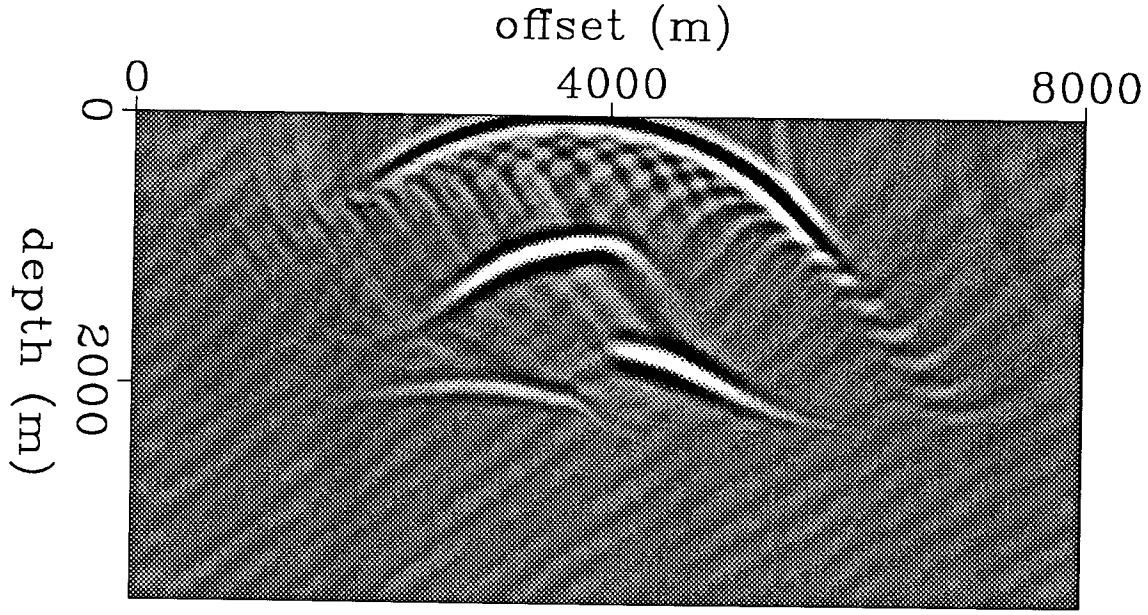

FIG. 25. S_h wave field propagating in reverse time using the anisotropic elastic S_h wave equation.

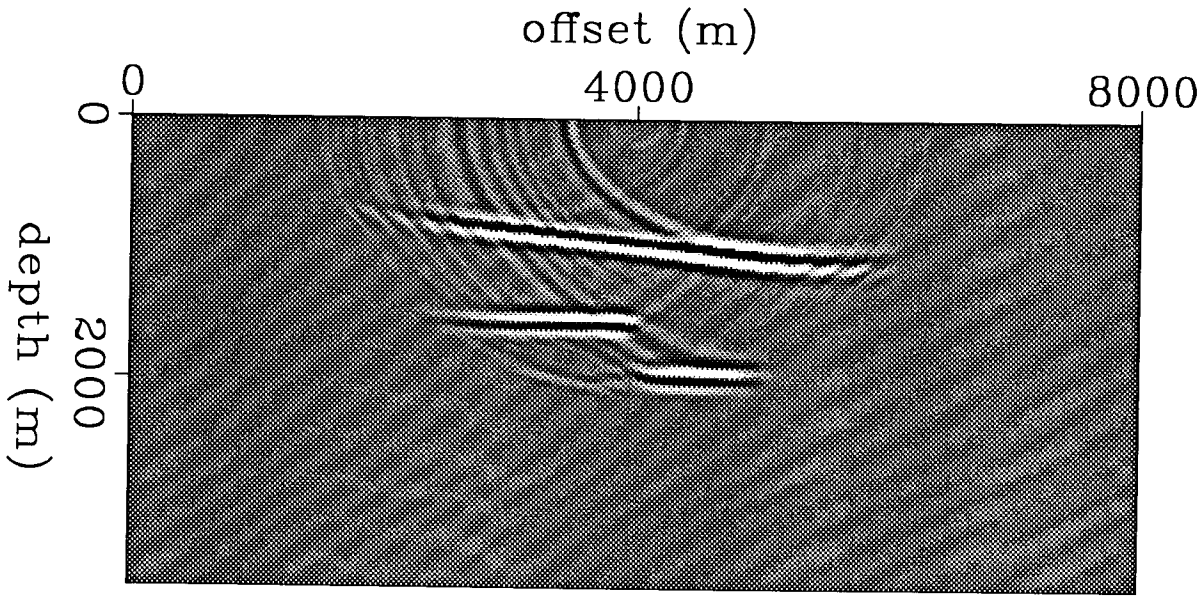

FIG. 26. Prestack depth migrated image obtained using the anisotropic elastic S_h wave equation. The reflectors are correctly imaged.

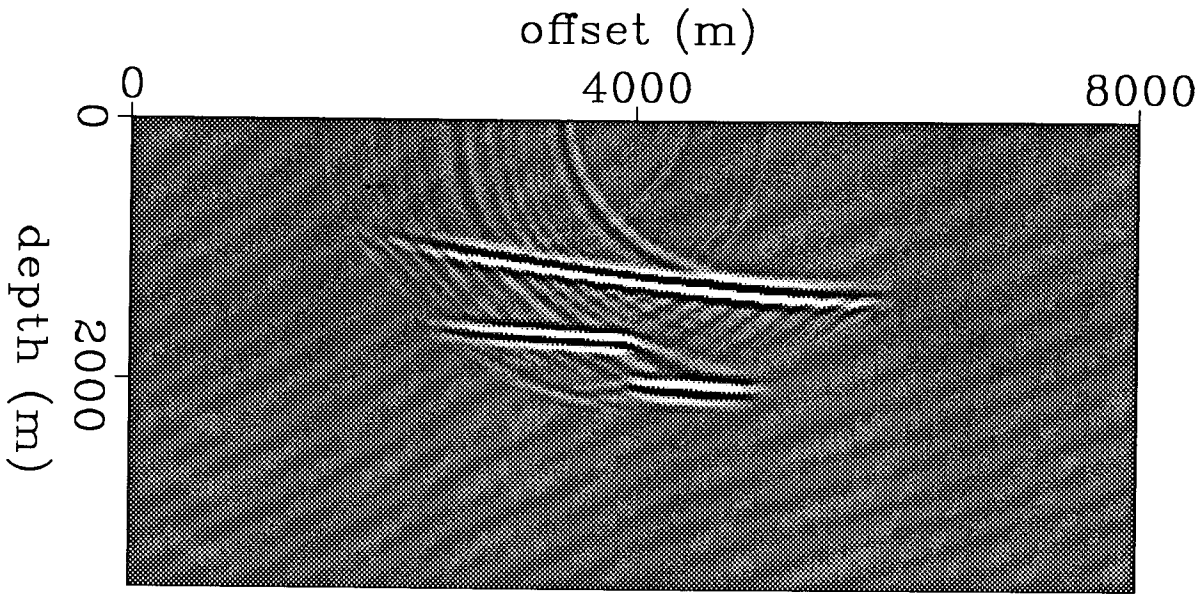

FIG. 27. Prestack migrated image obtained using the isotropic elastic S_h wave equation. The velocity used for back propagation was the horizontal S_h wave velocity. The image is not correct; the dipping bed is imaged too deep and the faulted bed should be flat.

Kosloff, D., Reshef, M., and Loewenthal, D., 1984, Elastic wave calculations by the Fourier method: Bull., Seis. Soc. Am., **74**, 875-891.

Kosloff, D., Reshef, M., Edwards, M., and Hsiung, C., 1985, Elastic 3-D forward modeling by the Fourier method: Presented at the 55th Annual Meeting of the Society of Exploration Geophysicists, Washington D. C.

Marfurt, K. J., 1984, Accuracy of finite-difference and finite-element modeling of the scalar and elastic wave equations: Geophysics, **49**, 533-549.

Mora, P., 1986a, Elastic finite-differences with convolutional operators: SEP-48, 151-169.

Mora, P., 1986b, Nonlinear 2D elastic inversion of multi-offset seismic data: SEP-48, 151-169.

Sword, C., H., 1987, Numerical dispersion and attenuation in the M3 modeling system: SEP-56, 1-18.

Vidale, J. E. and Clayton, R. W., 1986, A Stable free surface boundary condition to two-dimensional elastic finite-difference wave simulation: Geophysics, **51**, 2247-2249.

Virieux, J., 1986, P-SV wave propagation in heterogeneous media: Velocity-stress finite-difference method: Geophysics, **51**, 889-901.

Virieux, J., 1984, SH wave propagation in heterogeneous media: Velocity-stress finite-difference method: Geophysics, **49**, 1933-1937.

Fault line study shakes up views of quakes' causes

By JOEL SHURKIN

Geologists studying California have found that the amount of stress on the dangerous San Andreas fault is far less than they have believed it to be.

The theory does not mean the fault is less perilous, only that it takes less stress to trigger an earthquake, says Stanford geophysics Prof. Mark Zoback. It could, however, give scientists crucial information about how the fault operates that could help geologists predict quakes.

"It's a whole new ballgame in discussing fault zone propagation," Zoback says. The theory also explains a number of geologic features on the California coast that had puzzled geophysicists.

Zoback and several others have submitted their finding to *Science*, the journal of the American Association for the Advancement of Science.

The data for the paper came from two sources, Zoback says: information from boreholes and earthquakes in central California, away from the San Andreas, and a deep drilling project Zoback and other geologists are operating near the fault at Cajon Pass in the San Bernardino Mountains.

The San Andreas is a large fault line that delineates the boundary between two huge continental plates, the Pacific and the North American. It runs from offshore, north of San Francisco, through the central coast and Southern California into Mexico.

Its most famous activity was the 1906 earthquake that triggered the fire that destroyed San Francisco. Geologists believe the San Andreas is coiled to jolt again soon, particularly in Southern California.

The research by Zoback and his colleagues, however, was instigated by a major inconsistency in data about the fault: If there is a great deal of stress on the fault, why isn't there a great deal of friction heat along the fault?

"We've been arguing about the magnitude of stresses on the fault; in other words, how much force does it take to cause the fault to move?" Zoback says. "This argument has been going on for 20 years because the rock mechanics information we have from laboratory studies and the theoretical studies of faulting all predicted that the stresses would be high."

Additionally, quakes along the fault should be relieving much more stress than geologists have measured, he says.

"The amount of seismic radiation tells us about how much stress is being relieved . . . and it wasn't very much. That's what got us into the project."

Zoback and geophysicists from the U.S. Geological Survey and other universities around the country are drilling near the San Andreas in the Cajon Pass, using one of the largest oil well drilling rigs in North America. The hole they are drilling will be the deepest ever dug outside the Soviet Union for scientific purposes.

They reached a depth of a little more than 2 kilometers (about 7,000 feet) before drilling was suspended in the spring. They hope to resume drilling to 5 kilometers in the autumn.

But preliminary results from the Cajon Pass experiment have confirmed that there is almost no stress acting along the fault. That led Zoback and the others to look for data away from the fault.

"One reason why this eluded us for so long is that, when we think about stress on the San Andreas, we basically always think about what the San Andreas itself was telling us; but the trick was to get enough data adjacent to the fault that we could essentially ignore the San Andreas and look at the stress causing it to move," he said.

That meant going through data collected by many geologists in California's Central Valley region, both from earthquakes and from holes drilled for oil and other reasons.

"Suddenly, now our Cajon Pass project is tied to the whole geologic fabric of central California, and it's all wrapped up in one nice little story: The San Andreas is extremely weak."

They found that the evidence for this theory had been staring geologists in the face all the time. All they needed to do was look at the Coast Ranges of mountains.

The Coast Ranges run all along the western boundary of the United States down to Santa Barbara and include the Santa Cruz and Diablo mountains in the Stanford area.

"The striking thing about the Coast Ranges is that they have come up pretty fast, basically in the last four million years or so. Things along the San Andreas haven't really changed very much in the last four million years, so why did the Coast Ranges pop up?" This anomaly was first noted by Stanford geophysicist Ben Page, Zoback says.

"Associated with the Coast Ranges are a bunch of folds and faults, all of which, taken together — both onshore and offshore — indicate that the earth is being stressed in a kind of northeast-southwest direction, perpendicular to the San Andreas fault."

This is important, Zoback maintains, because it reflects on the orientation of the stress along the fault — the way the crust is being pushed and pulled.

If the fault is very weak, he says, the orientation of the stress has to be in one of two directions, almost perpendicular to the fault or almost parallel to it.

"This is sort of an obvious point that essentially escaped all of us until recently," he says.

"If the fault is very weak, the stresses cannot be oriented in such a way that they generate a lot of stress on the fault. You can't put more stress onto the fault than it can withstand."

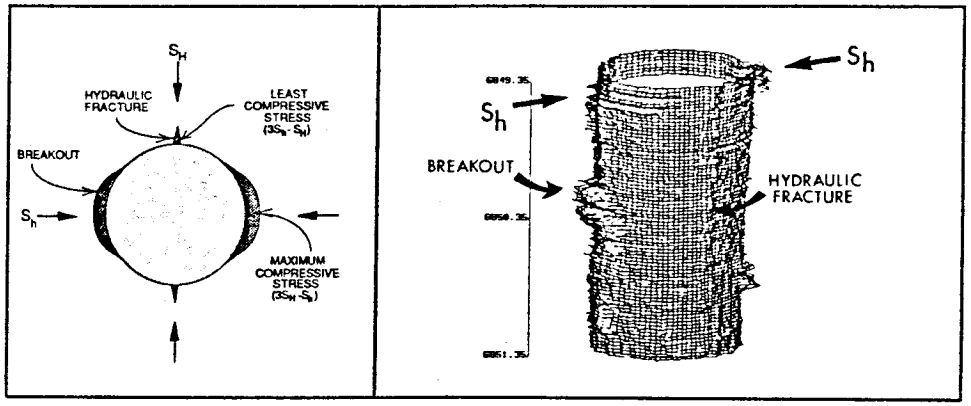

A three-dimensional computer image of a section of the Cajon Pass well bore. Water is forced into the bore to find the fractures in the rocks, both natural and induced

The data that led to the next stop already were available from work done in central California. They indicated that the current stress adjacent to the San Andreas was nearly perpendicular to the fault, and if the San Andreas was moving in such a stress field it could not be not very strong. That would explain the low heat within the fault, and the whole geology of western California.

To explain how this works, Zoback uses the analogy of a box on a floor. If you push down on the box from almost directly above, it will only move if the floor is very slippery. The fault, in this case, provides the slippery floor.

"We know the San Andreas is moving — we know the box on the floor is slipping away — but if we want to see the forces that are causing it, don't look at the thing that's slipping, look at the blocks adjacent to it. That was the key, getting the data outside of the boxes."

'Now our Cajon Pass project is tied to the whole geologic fabric of central California, and it's all wrapped up in one nice little story: The San Andreas is extremely weak'

The Pacific plate, which incidentally includes Los Angeles, is moving in a generally northerly direction; the North American, which holds San Francisco, moves south. (Some day, in years measured in the millions, the sites of the two cities will pass.)

But the Pacific plate also has a very slight convergent motion eastward.

"That's existed for the last four or five million years," Zoback says. "Prior to that, the relative motion of the Pacific plate was the other way. That doesn't seem like any big deal, but . . . the fault is so weak and the maximum stress direction either has to be perpendicular or parallel to the fault so the fault acts like a stress amplifier, amplifying distant plate motions."

During this earlier period, the offshore and inland basins of California were being formed. Then, "pow, four or five million years ago everything changes by 90 degrees, and we go through this remarkable period of uplift and folding. You get a 90 degree change in orientation. Stresses [are] such that those very young sediments — only five million years old, and . . . deposited in some nice little basin five million years ago — found themselves being uplifted into the Santa Cruz Mountains."

This relatively small change in motion was amplified by the weak fault cutting through the earth's crust, he says.

"It really has dramatic geologic consequences.

"Weak simply tells us the amount of force required to make it move. It moves nonetheless; the amount of seismic energy that's released is the same. But the other important consequence of the weak fault is that the composition of the fault has to be much different than the simple models and the laboratory analyses. . . .

"The fault has to have a very unusual . . . behavior. The laws which govern its deformation are very unusual and not at all predicted by the majority of simple laboratory studies that have been done to date.

"Now this makes us go right to the heart of the earthquake process. It begs really important questions about exactly what happens in the strain accumulation and what is the gouge [pulverized rock largely altered to clay in the fault].

"The fun part of it is that, in retrospect, the implications of the lower stress model should have been clear to us before. But now, being confronted with the evidence, the implications are really quite dramatic and exciting and give us a kind of new way of viewing things we see in geology.

"Suddenly, we say that the forces are perfectly oriented to explain the geology, which is kind of neat. Suddenly, all this obvious geology is related to a mechanism."

Several other Stanford professors are participating in the Cajon Pass experiment. Amos Nur and Michael McWilliams of geophysics and their graduate students are examining core samples. Irwin Remson of applied earth sciences and his students are describing hydrology in the area.